THE UNIVERSITY OF ALBERTA

A MICROMETEOROLOGICAL STUDY OF AN URBAN VALLEY

by

© ROBERT DOUGLAS PATERSON

A THESIS

SUBMITTED TO THE FACULTY OF GRADUATE STUDIES AND RESEARCH

IN PARTIAL FULFILMENT OF THE REQUIREMENTS FOR THE DEGREE

OF MASTER OF SCIENCE

IN

METEOROLOGY

DEPARTMENT OF GEOGRAPHY

EDMONTON, ALBERTA

FALL, 1978

ABSTRACT

On the evening of the 21 October 1977 an experiment was run in a cross-section of an east-west segment of the North Saskatchewan River Valley in Edmonton Alberta. Measurements of temperature, wind, and carbon monoxide concentration were made in an attempt to determine the micrometeorology of the valley.

The inversion in the valley was more intense than in the city which is situated on the plain. The south side of the valley was colder than the north side, and its temperatures were comparable to a rural station.

Drainage winds were experienced on the slopes of the valley. The along-valley wind shifted from easterly to westerly as the inversion formed. During this time the prevailing wind remained southeasterly. A 15 minute periodicity in the drainage wind on the south side of the valley was determined by spectral analysis.

Carbon monoxide concentrations were found to be strongly influenced by the drainage wind, with a peak in concentration three hours after the late afternoon rush-hour traffic maximum.

The data were not of sufficient resolution to describe the complete valley wind circulation, but the potential for pollutant entrapment within the valley was established.

ACKNOWLEDGEMENTS

I wish to express my gratitude to my departmental supervisor, Dr. K.D. Hage, for having suggested this study and for his advice on procedures of analysis. My thanks are extended also to Dr. R.B. Charlton and Dr. A.K. Hellom who along with Dr. Hage served on my examining committee.

I wish to thank Mr. R.P. Weatherburn for his advice and assistance in the organization and operation of the experiment on which this thesis was based, and all those people who manned the instrumented stations.

The cooperation of Dr. D.J. Wilson in the operation of the Mechanical Engineering Low Speed Wind Tunnel was greatly appreciated.

Financial support for this project was provided by the Research Secretariat of Alberta Environment under contract #AE 77-72.

This study was conducted while on Educational Leave from the Atmospheric Environment Service, Fisheries and Environment Canada.

TABLE OF CONTENTS

LIST OF TABLES

LIST OF FIGURES

CHAPTER 1

INTRODUCTION

1.1 Reasons for the Study

Many cities the world over are built around small river systems, where the river valley is below the level of the city. In many cases, these valleys are used for public recreation, including parks, amusement areas and recreational boating. These valleys are then at times the location for large congregations of people, which in turn leads to high levels of motor vehicle activity in access roads and parking lots. Those areas of the valley not used for recreation are often sites for major urban roads and freeways, as well as various types of commerical enterprise. Due to the small size of these valleys, the concentration of pollutants would not be expected to be of concern during the day when thermal mixing processes transport the pollutants out of the valley, but what of the night? Especially during the summer, evenings are when the maximum concentration of people would be expected and when the formation of inversion conditions would be most likely to concentrate the pollutants in the river valley. The questions arise: will the inversion conditions formed in these small river valleys be independent of the larger urban environment?; how will the urban environment

affect the river valley?; will the circulation within the valley be a closed system? There seems to be few studies that have concerned themselves with the micrometeorology of small urban valleys, but perhaps some of the observed circulations in large mountain and river valleys would apply to the small river valleys.

The phenomenon of mountain and valley winds has been investigated by Geiger (1965), Defant (1951) and others. Observation shows that well-developed local circulations with marked diurnal variations are formed in valleys leading into mountain ranges. There is a double system of periodic winds; during the day there are upslope and upvalley winds and at night downslope winds and downvalley winds. The slope winds are always initiated first and the valley winds follow. An idealized description of valley winds is given by Defant (1951), (Fig. 1.1): At sunrise upslope winds begin (white arrows), but the valley is still colder than the plains and the downvalley winds (black arrows) are still blowing, fed by return circulation from the slopes. It soon dies out with further heating. In the forenoon (B), the slope winds are strong and there is a transition from a mountain wind to a valley wind, with the valley and plains temperatures the same. By noon and early afternoon (C) the slope winds are diminishing and there is a fully-developed valley wind, with the valley warmer than the plains. In the late afternoon (D) the slope winds have ceased and the valley wind continues. In

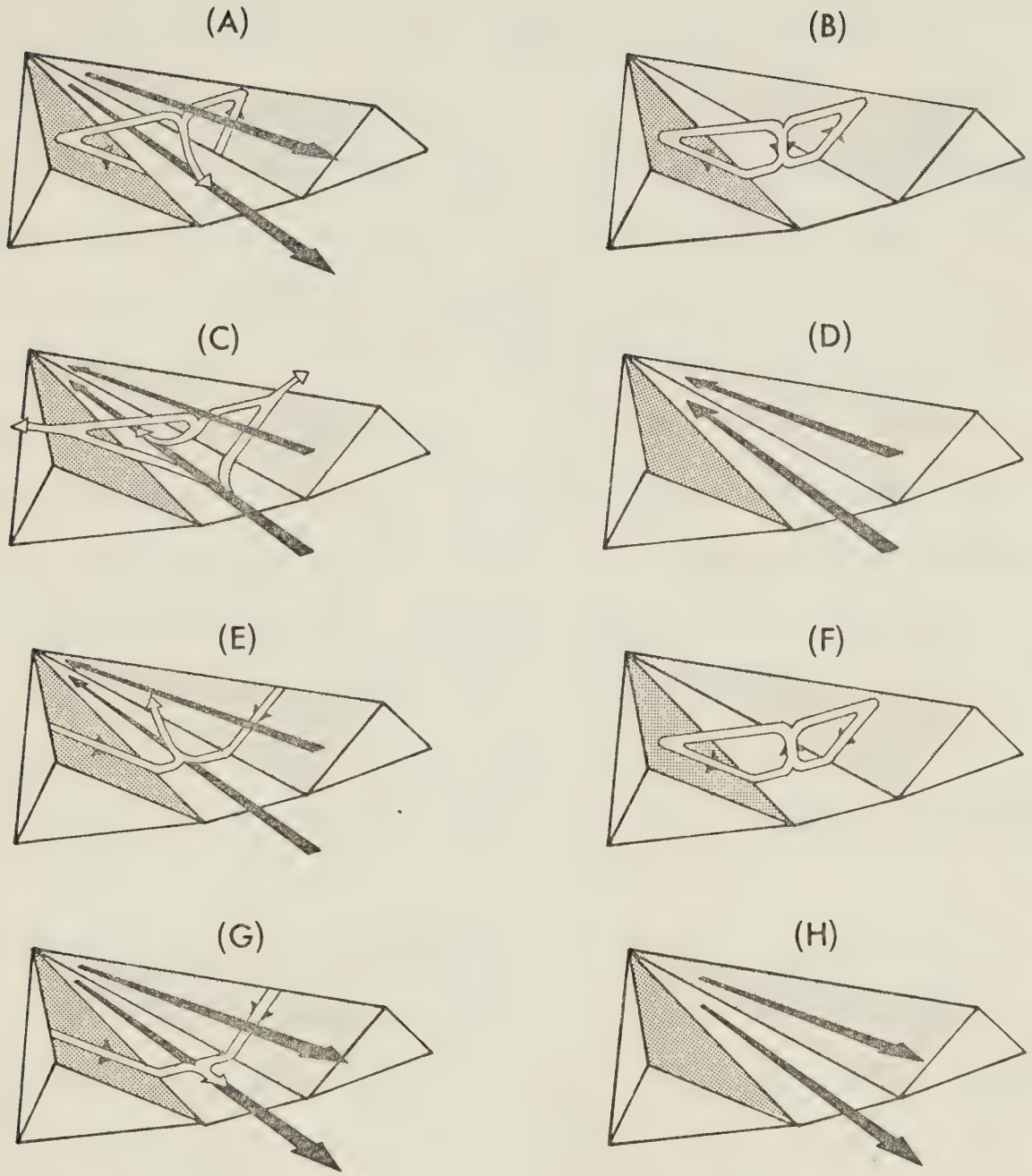

Fig. 1.1. Schematic illustration of the normal variations of the circulation in a valley (after Defant, 1951).

the evening (E) downslope winds begin and the valley winds diminish. The valley at this time is only slightly warmer than the plains. By early night (F) there are well-developed downslope winds and a transition from a valley wind to a mountain wind. The valley and plains are at the same temperature. The middle of the night (G) sees the mountain wind fully developed, with the valley colder than the plains and by late night (H) the downslope wind has ceased and the mountain wind fills the valley. This description of the progression of the valley winds will be further complicated if there is a cross-valley prevailing wind (Tang, 1975), which may result in closed cell (cut off) circulations. This then forms the basis on which to begin the investigation of small urban river valley circulation and gain an insight into possible pollution problems.

1.2 Edmonton's River Valley

Within the City of Edmonton (53°33'N, 113°30'W) the dominant topographical feature is the North Saskatchewan River Valley. A large part of this valley is used for public recreational activities and includes much of the city's parkland. For this reason it is of interest to study the valley microclimate and pollution potential and if possible develop simulation (computer) models. Within the valley are complex arrangements of motor vehicle pollution sources with bridges (cross-valley line sources), streets and roads (along-valley line sources) and parks

and residential districts (area sources). This valley is known to possess its own microclimate, with, for example, minimum observed temperatures on clear nights on the floor of the valley comparable to those reported at nearby rural stations (Hage, 1972). Evidence for poor mixing within the river valley is occasionally seen in fog situations where the layered nature of the fog is indicative of the absence of effective mixing between valley and plains air. Klassen (1962) found that the river valley system in Edmonton simulates the description of the model suggested by Defant (1951), but he did not observe an upvalley wind which was independent of the prevailing airflow. He observed a downslope wind under conditions of clear skies and light prevailing wind and found the downslope flow to be weak, very unsteady and quite shallow. Air was seen to flow down the valley even when the prevailing wind blew perpendicularly across the valley. It was suggested that a double-vortex circulation develops under favorable conditions, with ascent over the relatively warm river water and descent along the slopes.

In an attempt to answer some questions on the circulation within the valley, field experiments were run within the river valley in the center of Edmonton. Measurements of wind, temperature and carbon monoxide concentrations were made.

CHAPTER 2

EXPERIMENTAL LOCATION AND INSTRUMENTATION

2.1 Topography

The City of Edmonton is located on the banks of the North Saskatchewan River in central Alberta. Edmonton lies 670 m above sea level on a plain that slopes gently from the southwest down to the northeast (Fig. 2.1). The North Saskatchewan River meanders through Edmonton from the southwest to the northeast and the valley is steep sided and narrow, with an average depth of 50 m. The width of the valley varies from 1000 m in the straighter sections to 1500 m. Data were collected from the Edmonton City Tower (A), the Municipal Airport (YXD), the International Airport (YEG) and mainly from the High Level Bridge (B) area. The International Airport is situated 32 km due south of Edmonton in a rural setting.

The detailed study of the river valley was done in a cross section of the valley in the vicinity of the High Level Bridge (Fig. 2.2). The bridge consists of two traffic levels with a railbed on top and a motor vehicle roadway below. Pedestrian walkways are found on both sides of the roadway. The walkways are 42 m above the river. The south slope of the river valley in the area of the bridge has no major roads running parallel to the river and no through

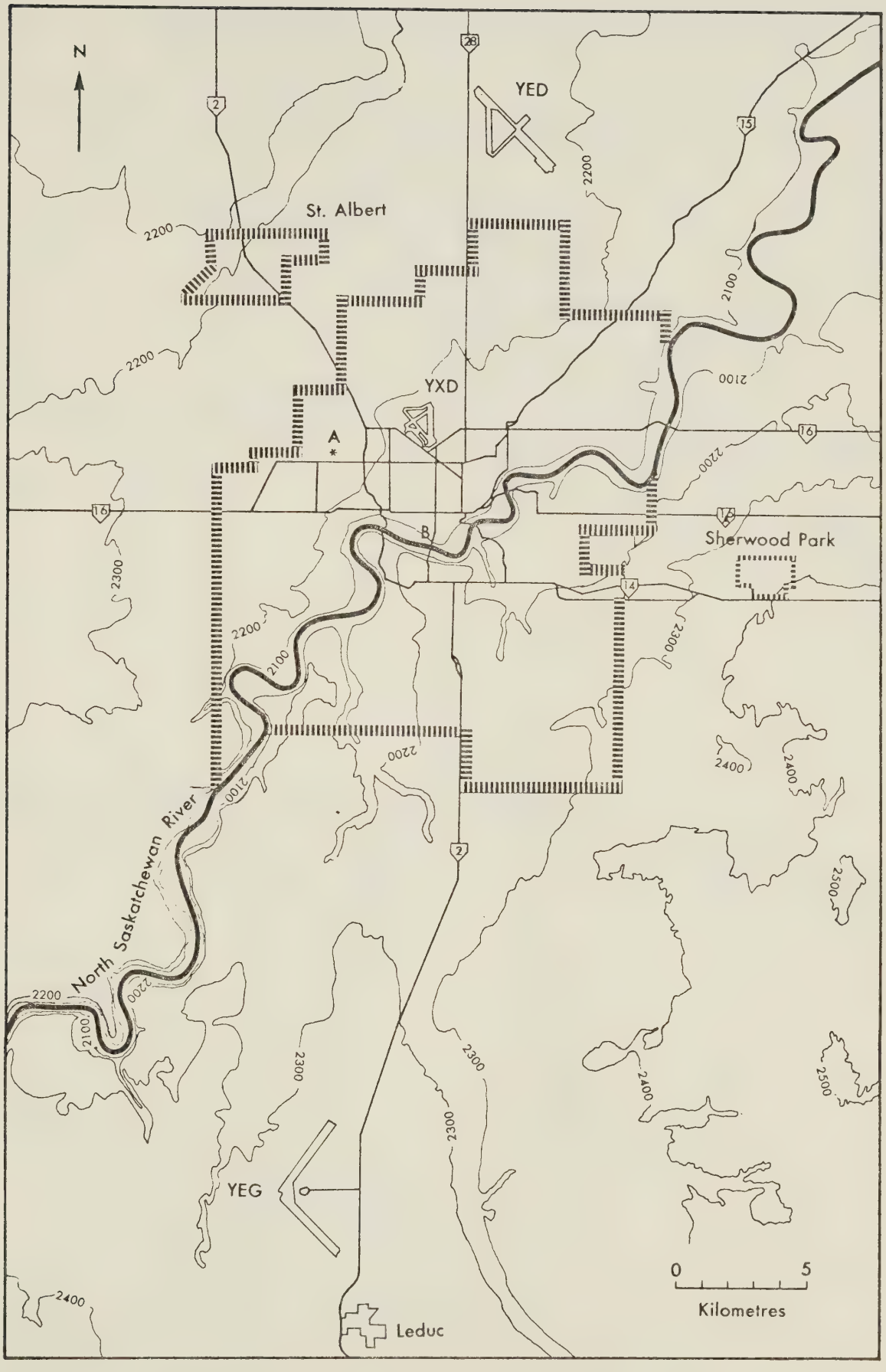

Fig. 2.1. Map of Edmonton, Alberta, and vicinity. Contours in feet at 100' intervals.

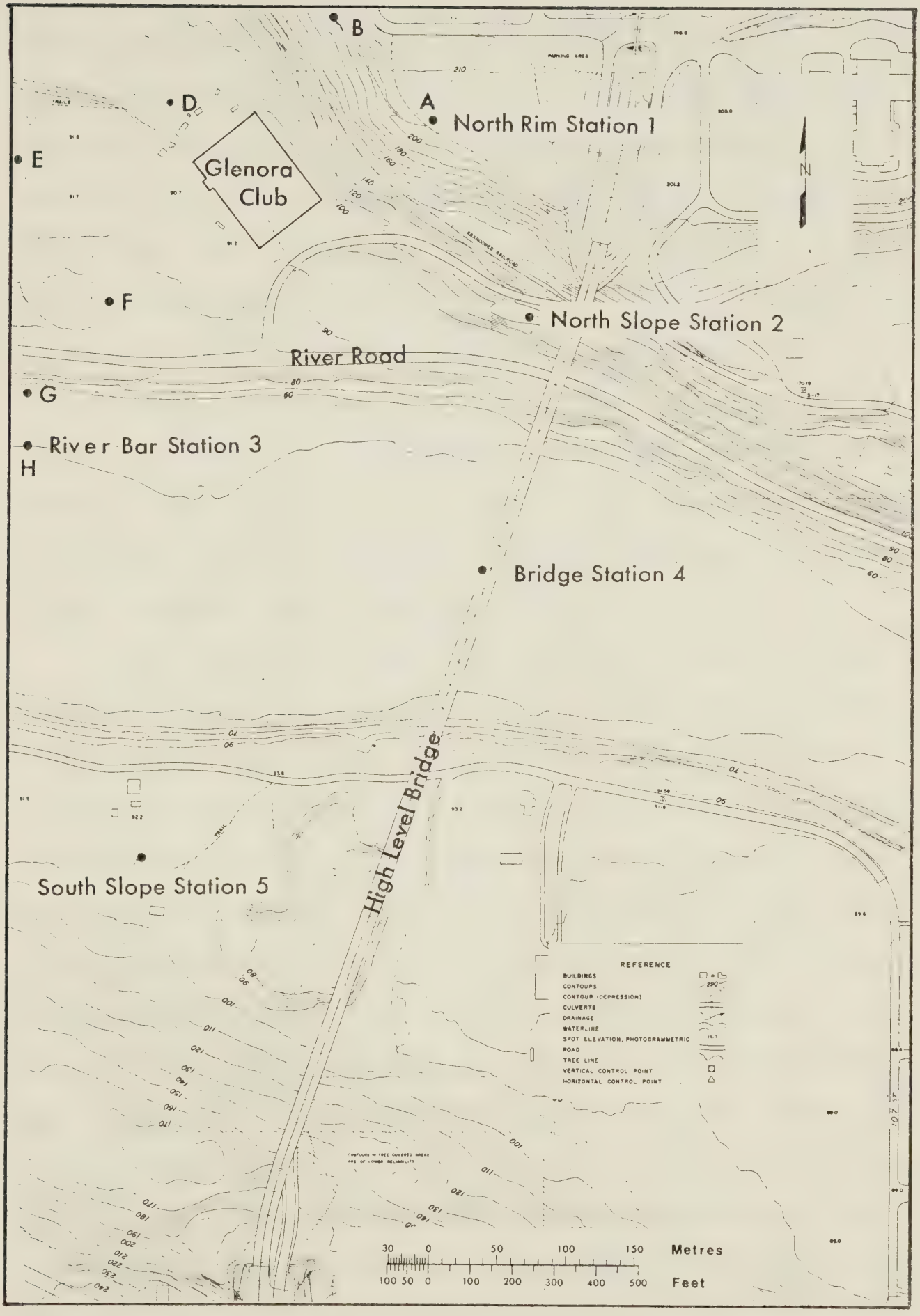

Fig. 2.2. Location of Instrumented Stations. Contours in feet at 2' intervals.

roads west of the bridge below the rim of the valley. The south slope is heavily treed. The north slope vegetation consists of tall grasses and is sloped more steeply than the south slope. River Road is a major traffic artery within the city. The road down the north slope passing under the bridge is lightly travelled. Traffic counts along River Road vary from 1,700 motor vehicles per hour at 1700 MDT to 200 per hour at 0100 MDT. The south rim is level and there are large high-rise buildings running for most of its length in the vicinity of the High Level Bridge. The north rim of the valley is a large open area of short grass, with no nearby large buildings.

The locations of the experimental stations are indicated in Fig. 2.2. The numbers 1 to 5 indicate the locations of the main fixed experimental stations and the letters A to H indicate the locations of the carbon monoxide monitoring stations. Stations 6 and C are not indicated as both were located beyond the area covered in Fig. 2.2. Station 6 was located on the south rim of the valley about 0.5 km west of the bridge and station C was located at the base of the north slope WNW of station D. The elevations of the main stations (1-6) are indicated in the cross section of the river valley 40 m west of the High Level Bridge (Fig. 2.3). Stations 4a to 4d indicate the locations of a thermocouple array that was suspended from the High Level Bridge.

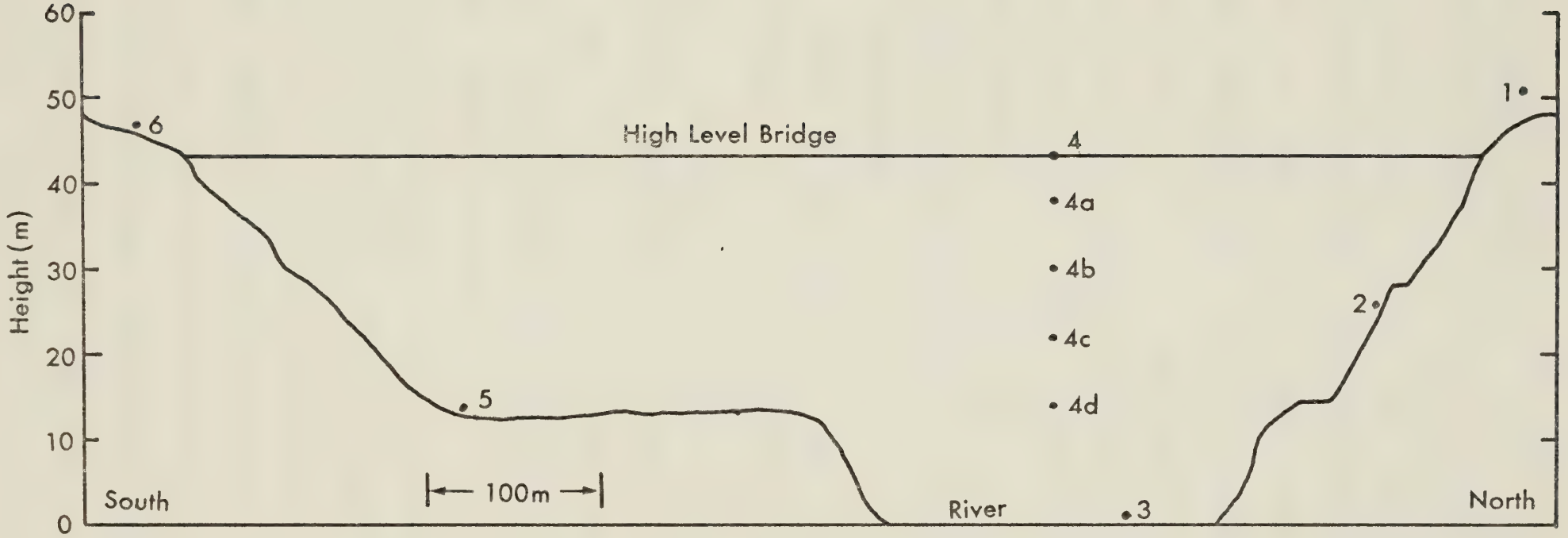

Fig. 2.3. Cross section of North Saskatchewan River Valley 40 m west of the High Level Bridge. Numbers refer to instrumented stations. Vertical exaggeration 5x.

2.2 Experimental History

During the summer and fall of 1977, experiments were run to provide data for modelling studies. Temperature, wind and carbon monoxide concentrations were measured under light winds and clear skies. Thus the microclimate of the valley was observed under inversion conditions. The first experiment, run on July 13, was a preliminary study to gain familiarity with equipment and to establish procedures. The second experiment, run on July 20, did not yield light winds, and the mean wind penetrated to the floor of the valley. The third experiment held on July 26 gave the required conditions.

It became obvious that more was occurring in the micrometeorology of this small valley than had been expected and, in many respects, the findings resembled those for larger valleys. A survey of the literature did not reveal any work done on this scale of river valley, although many studies had concerned themselves with mountain valleys or large river valley systems.

To investigate the observed complexity, additional instrumentation was obtained or designed to allow study at locations where only battery power could be used. As very light winds had been observed previously, this equipment also had to have good sensitivity and stability.

A fourth experiment was run on October 21, during the period of 1800-2400 MDT, although some stations have slightly longer records. Additional information was gained from the

Municipal Airport, the International Airport and the Edmonton City Tower.

2.3 Station Instrumentation for Experiment 4

The positions available for the stations were all easily accessible by the public, as much of the river valley is part of the regional parks system. As a result all stations were manned continuously and all equipment was removed at the end of each experiment. Portable meters[1] were used for the measurement of carbon monoxide concentrations and the output recorded on portable chart recorders.[2] The meters and recorders were carried from station to station and five minute readings of concentration were taken at each station. The instrumentation which was located at each station is listed in Table 2.1. All thermographs were held in Stevenson screens, with those at stations 1 and 3 suspended above the ground, those at stations 2 and 6 placed on the ground and the screen at station 5 was placed on a picnic table. Temperature profiles were obtained at station 4 by suspending thermocouples from the bridge at 5, 13, 21 and 29 m below the road level of the bridge. The anemometers at stations 1 and 3 were supported by standard television antenna tower sections and the profiling anemometers at station 2 were

---

[1] Interscan Corporation model no. 1148.

[2] Esterline Angus Corporation model no. MSH401BB.

Table 2.1. Meteorological Instrumentation

Station	Variable	Instruments
1	wind speed and direction	cup and vane anemometer
	air temperature	thermograph
2	slope wind	propeller anemometer
	wind profile	cup anemometer
	air temperature	thermograph
3	3 wind components	propeller anemometers
	wind profile	cup anemometers
	air temperature	thermograph
	water temperature	thermograph
4	bridge level air temperature	thermister
	4 level air temperature	thermocouples
5	slope wind speed	propeller anemometer
	wind direction	vane
	air temperature	thermograph
6	air temperature	thermograph

supported by a guyed metal tube. The propeller anemometers at the river valley slope stations 2 and 5 were aligned along the slope so as to measure the up and down slope component of the wind. The heights above ground of all instruments are listed in Table 2.2.

2.4 Calibration

The thermographs used were made by Casella, Thies and Ryan Instruments,[1] the latter being submersible for obtaining water temperatures. Measurements of temperature at station 4 were obtained from a thermister thermometer.[2] This thermometer was found to be accurate when calibrated against a standard mercury-in-glass thermometer and was used as a reference for all other instruments because of its rugged portability. Profile measurements were made by thermocouples of nickel-constantan of 0.013 mm diameter. This size was used to avoid radiation effects, as the elements could not be shielded. The output from the thermocouples was measured by a digital readout[3] which was not capable of reading below a machine reading of 0°C. Calibration of the temperature measuring instruments was carried out at several temperatures, using both the Meteorological Division cold room and

---

[1] Ryan Instruments model no. F-8.

[2] Weather Measure Corporation model no. T618-1-B.

[3] Omega Engineering model no. 200-EC2-DSS.

Table 2.2. Height of instruments above ground.

Instrument	Station	Height (m)
thermograph	1, 3	1.5
	1, 6	0.15
	5	0.9
cup anemometers	1	4.1
	2	1.0, 2.0, 3.0
	3	2.6, 1.4
propeller anemometers	2	0.78
	3	4.5
	5	0.53
vanes	1	4.1
	5	0.6

still outside air, over a temperature range of +20°C to -15°C. Many of the instruments used had slight temperature dependencies and for these regression lines were fitted to the calibration points. Accuracy of the thermographs was affected by two factors: the extraction of data from the charts, and the slightly differing positions of the paper on the recorder drum. Data could be extracted from the chart itself to within 0.1°C and the positioning error can be inferred from the average standard error of regression, which was about 0.2°C, implying a position error of about 0.1°C. The thermister thermometer could be read to within 0.1°C and the digital readout for the thermocouples is specified to within 0.1°C resolution.

Impulse counting anemometers[4] were used to obtain wind profiles and a cup anemometer and chart recorder system[5] was used at station 1 to measure prevailing wind. All propellers were of the Gill type. Anemometer calibration was carried out in the University of Alberta Mechanical Engineering Department low speed wind tunnel, which is capable of speeds down to 0.04 m s^{-1}. The calibration reference for the speed range of 0.05 to 2.0 m s^{-1} was a hot film anemometer owned by the Mechanical Engineering Department and which was calibrated from first principles and linearized

---

[4] Rimco C.S.I.R.O. model ASI.

[5] R.M. White anemometer model no. 5-902, recorder model no. 1-188.

over this range. Above 2 m s^{-1} the Gill propeller anemometers were used as a reference as the response was found to be linear above 1 m s^{-1}. The stall speed of the R.M. White cup was found to be 1.5 m s^{-1}. The Gill anemometers were very close to one another in calibration and stall speed, the latter varying from 0.15 to 0.18 m s^{-1}. The counting cup anemometers also proved reasonably sensitive with stall speeds grouped about 0.32 m s^{-1}.

The zero calibration of the carbon monoxide meters was found to be unreliable, so to detect zero drift, the meters were left to run continuously for the duration of the experiment. In this way the zero drift could be observed and corrected for, as the drift was relatively slow and steady.

2.5 Chart Recorder Design

During analysis of Experiment 3, it became obvious that a sensitive chart recorder was needed to obtain satisfactory resolution of wind speed, which could change by an order of magnitude or more during the period of interest. Due to site location, the recorders had to be light and battery powered, since none of the sites had access to commercial power lines. As Rustrak[6] chart recorders were available, it was decided to design electronics for these recorders. The Rustrak recorders consist of a one milliampere meter movement, whose indicating arm can be clamped

---

[6] Rustrak Instrument Company model no. 214C.

by a striker bar to mark pressure sensitive chart paper. The chart paper is driven by a 12 volt d.c. motor, which also controls the striker bar. The drain of this motor is very low, so that the current drain on the 12 volt lantern battery used will not reduce the output voltage by a measurable amount by the end of the experiment. Depending on the gear train selected, speeds of up to 30.5 cm hr^{-1} (12 inches hr^{-1}) could be obtained. During Experiment 4, station 5 used a chart speed of 15.25 cm hr^{-1} (6 inches hr^{-1}) and all other stations used 30.5 cm hr^{-1}.

Operational amplifiers were selected for the chart recorder electronics due to their precisely-defined parameters and ease of replacement in the event of failure. Originally only 741 type operational amplifiers were used, but due to their high input bias requirements of 2×10^{-7} amperes, any change in the input or feedback loop impedance caused large changes in the output offset. No rearrangement could cure this problem due to the change of three orders of magnitude in input impedance shown by the required input attenuater. After some experimentation it was decided to use the National Semiconducter LM310N as an input buffer. This amplifier has a typical input bias current of 1×10^{-9} amperes and isolates the 741 from impedance changes. The current feedback loop around the 741 (Fig. 2.4) was found to provide the most stable operating point, with no instabilities developing and with no discernible output zero drift after several hours.

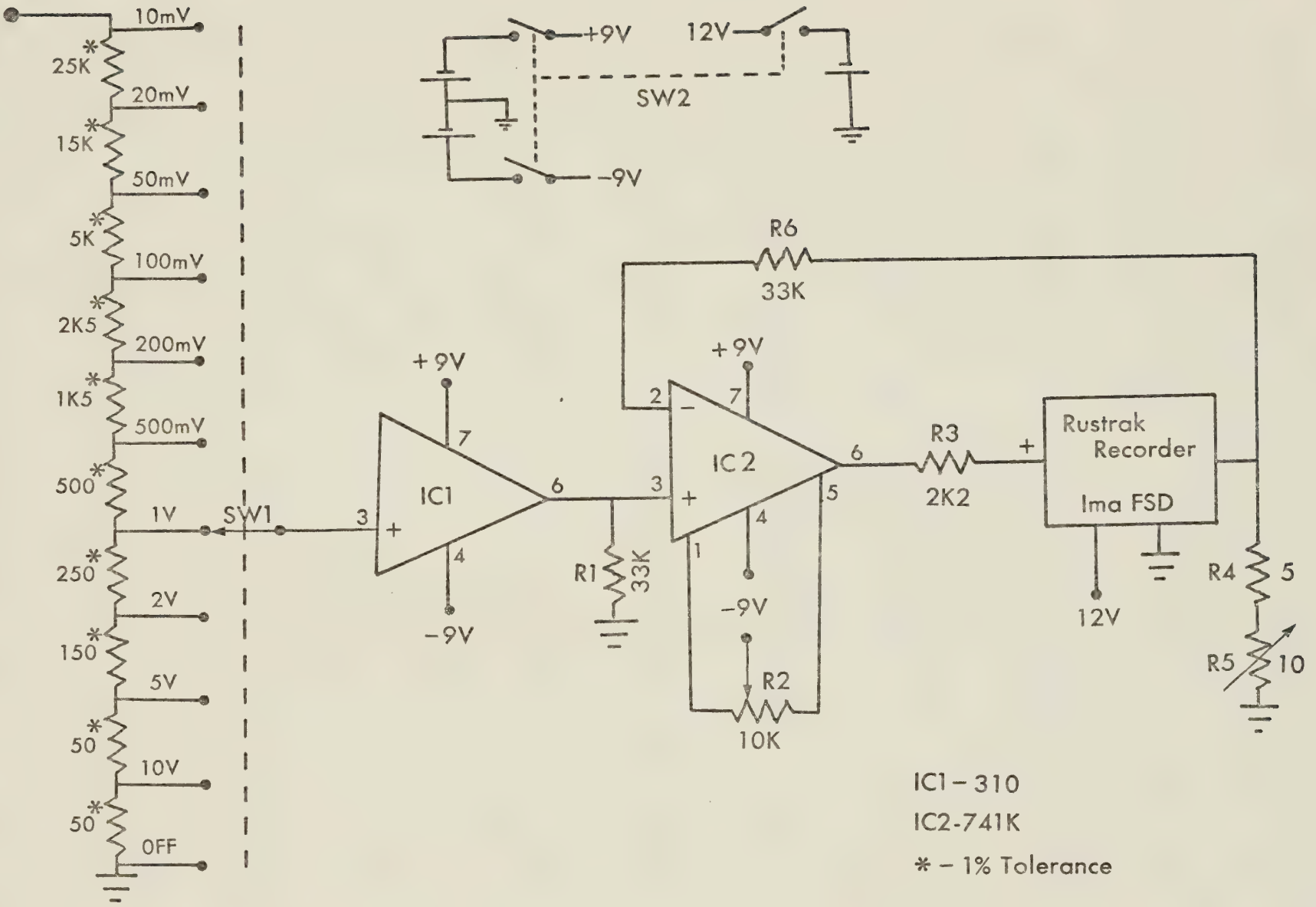

Fig. 2.4. Circuit diagram of chart recorder. Switch SW1 is a make before break. All resistors 5% tolerance unless noted.

As shown in the circuit diagram, SW1 is the input attenuater, stepped in a semi-logarathmic sequence and providing a constant input impedance of 50 KΩ, as the shunt impedance of the LM310N is 1.5×10^{10} ohms. All resistors in the attenuater are one percent metal film resistors for best stability and accurate input attenuation. The large range of input voltages available, while unnecessary for Experiment 4, was designed to allow greater flexibility in future experiments. Resistor R3 limits the maximum current available to the chart recorder, should a device failure occur, to 4 milliamperes to prevent burning out the meter movement of the recorder. Output offset is controlled by variable resistor R2, in conjunction with the internal circuitry of the 741. Gain is set by resistors R4 and R5, with the maximum gain limited by R4 to two and the minimum gain limited by R4 and R5 in series to 0.7. Switch SW2 is the power on-off switch. There is interaction between the output offset control and the gain control. Changing the gain will change the offset, but the offset will not affect the gain. The initial set-up procedure consists of adjusting both gain and offset one after the other until the full-scale range is accurate. Once the full-scale reading is correct, the offset may be adjusted and the gain will not be affected. Gain stability depends on the stability of resistors R4 and R5 and output offset stability will depend on the stability of R2. The circuit is not voltage sensitive and will operate well at 7.5 volts. Total current draw

of the circuit at full scale deflection is 5.3 milliamperes from the positive supply rail and 4.3 milliamperes from the negative supply rail.

The performance of this design was tested on all ranges. From maximum to minimum gain, the zero offset varies by 0.5 percent and full scale accuracy is within 1.0 percent. Total error of any reading was 2 percent with all errors additive. If a limited number of closely spaced ranges were used, accuracy was typically within the 1 percent level. The circuit was also tested with a calibrated voltage source for temperature drift. Within the range of 0°C to +21°C no change in gain occurred.

CHAPTER 3

RESULTS OF TEMPERATURE MEASUREMENTS

3.1 Temperature Profiles

The temperature profiles obtained at station 4 were augmented by temperatures measured at stations 1 and 3. The assumption was made that at any given height in the valley, excluding the slopes, the temperatures would be uniform over the horizontal distances separating the stations. To extend the temperature profiles into the urban environment, temperature measurements from the 10 m (A), 45.7 m (B) and 91.5 m (C) levels on the Edmonton City Tower were used (Fig. 2.1). The actual temperatures could not be used as comparison of the tower temperatures with temperatures obtained from the municipal airport (YXD) during inversion and lapse conditions showed differences of up to two degrees between the two locations. That these temperature differences were due to location was demonstrated when periods of continuous rain were used for comparison. During such occurrences, temperatures over large areas can be expected to be uniform and in these cases the tower and YXD temperatures were in good agreement. The assumption was made that the shape of the temperature profile would be the same over the river valley as at the location of the Edmonton City Tower and that the shape of

the temperature profile would be maintained with respect to its height above ground. To relate the tower temperatures to temperatures measured at the river valley, an estimate of screen-level temperature expected from the tower profile was made by extrapolating the 10 m to 45.7 m temperature difference to screen-level. The expected screen-level temperature was then equated to the actual temperature at station 1 and the entire tower temperature profile adjusted by the amount of the difference obtained. The tower measurements of temperature were assigned to the same height above ground at station 1 as at the Edmonton City Tower location. Temperatures obtained at half hour intervals, including the altered tower and river water temperatures are listed in Table 3.1.

Temperature profiles plotted every hour from 1800 to 2400 MDT are shown in Fig. 3.1 and, as can be seen, the variation of the profiles with time is reasonable. At 1800 the profile within the valley was isothermal and temperatures decreased with height above the valley. This is reasonable as the valley at this time had been in shade longer than the air above the city. A peak in the temperature profiles at bridge level in this and other profiles was attributed to the thermal effect of the High Level Bridge and the traffic on it, as the thermometer was located on the downwind side of the bridge. The bridge level temperature was much larger than expected from the other profile temperatures (up to 1.5°C), as well as erratic, so it was not

Table 3.1. Temperatures at stations used in constructing profiles above North Saskatchewan River.

		Station							City Tower Level		
Time	Water	3	4d	4c	4b	4a	4	1	A	B	C
1730	4.9	10.1	10.0	10.0	9.9	10.1	11.0	11.0	11.0	10.4	9.5
1800	4.8	9.5	9.6	9.6	9.7	9.6	10.3	9.9	9.8	9.5	8.9
1830	4.8	8.2	8.8	8.8	8.7	8.6	8.8	8.7	8.7	8.7	8.4
1900	4.7	7.4	7.7	7.8	8.0	8.0	8.2	7.8	7.8	7.7	7.7
1930	4.6	6.9	7.1	7.2	7.2	7.1	7.7	7.2	7.3	7.6	8.4
2000	4.5	5.0	7.0	6.7	6.9	6.7	7.4	6.9	7.0	7.6	8.3
2030	4.5	3.4	4.5	5.6	5.5	6.5	7.0	6.2	6.4	6.9	7.9
2100	4.4	2.9	3.6	3.7	4.1	4.6	6.6	5.2	5.4	6.3	7.9
2130	4.3	1.9	3.1	3.5	3.7	3.5	4.5	4.7	5.0	6.2	7.9
2200	4.2	1.6	--	2.4	3.1	3.1	3.4	3.7	3.9	4.8	7.9
2230	4.2	1.1	--	--	--	--	--	3.2	3.4	4.2	6.4
2300	4.1	-.4	--	--	--	--	3.8	3.1	3.3	4.2	7.2
2330	4.0	-.6	--	--	--	--	2.2	2.8	3.2	4.6	6.8
2400	3.9	-.9	--	--	--	--	1.1	2.2	2.8	5.1	6.9

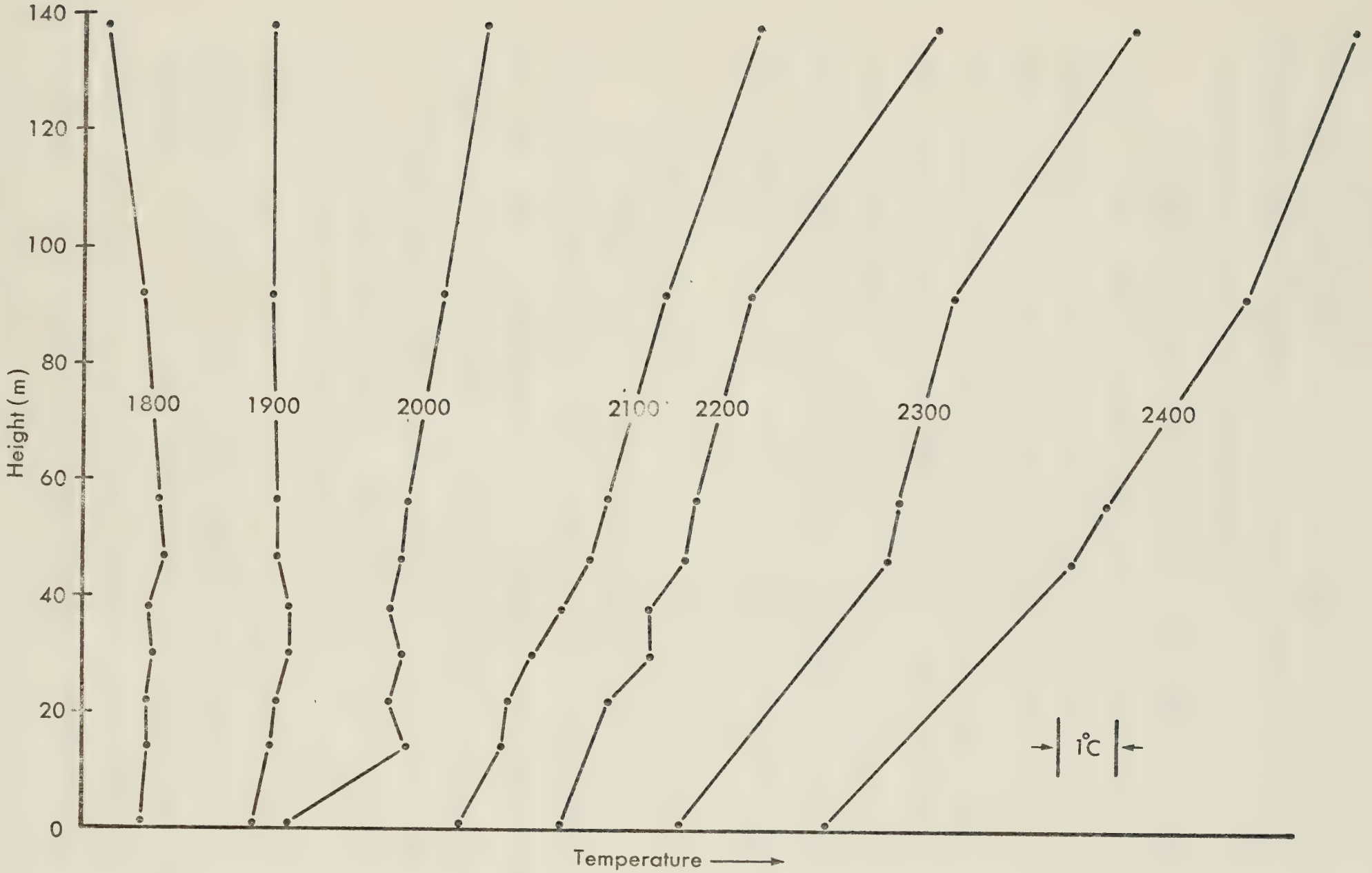

Fig. 3.1. Hourly temperature profiles within and above river valley.

included in the profiles. The thermometer was moved after 2100 to try and minimize the thermal effects, but the temperatures were still unreliable.

At 1900 cooling was evident in the lower 25 m of the river valley and the temperature profile above the city was isothermal. By 2000 the cooling in the lower levels of the valley was very pronounced and in later profiles this cooling had extended upward. Once the inversion had formed, the temperatures at the bottom of the river valley were always lower than would be expected from the Edmonton City Tower profile, indicating that the river valley may have been closer to a rural than to an urban temperature regime.

3.2 Time Variations

In order to follow the variation of temperature with time, the temperatures were plotted at ten minute intervals with the axis of one station plot shifted from another to illustrate the simultaneous time variations of temperature at all stations. The station temperatures used for the profile measurements within the valley are shown in Fig. 3.2. As can be seen, the onset of the inversion at station 3 was abrupt, starting after 1940 MDT. The temperature fell rapidly to a plateau at 2100. Rapid falls followed by a leveling off of the temperatures occurred three times before 2400. The inversion can be seen propagating upward through stations 4d to 4, marked by the tick marks in Fig. 3.2, at a constant rate of 0.7 m min^{-1}. The rapid drop in tempera-

Fig. 3.2. Time plot of temperature for river valley stations used in profiles. Numbers at beginning of plot indicate station. Tick marks indicate onset of inversion.

ture between 2100 and 2110 at station 4 was the result of moving the thermometer in an attempt to avoid the thermal effect of the High Level Bridge and was not an actual temperature decrease. The most probable real temperature trend is indicated by the dotted line. The initial accelerated drop in temperature at station 3 and the subsequent plateau was reflected in the temperatures of all other stations except station 1, indicating that this phenomenon was a characteristic of the river valley. The mechanism responsible for this behavior is at present unknown. The second rapid fall in temperature after the first plateau was again reflected in levels 4d to 4a, although not as clearly as the first decrease. The third rapid temperature fall at 2120 at station 3 was of greater magnitude than the second and was reflected in a rapid fall in temperature at station 4 one hour later than at station 3. This is in agreement with the upward propagation rate of the initial inversion which occurred at 1940.

The two slope stations 2 and 5, the south rim station 6, the municipal airport (YXD) and the international airport (YEG) temperatures are shown in Fig. 3.3 in the same form as in Fig. 3.2. Stations 5 and 6 showed no periods of rapid temperature decrease, but exhibited a steady cooling rate. The airport temperature showed large temperature changes from hour to hour, but the linear trend obtained with a least squares fit and indicated by a dotted line, showed general agreement with the cooling rates of

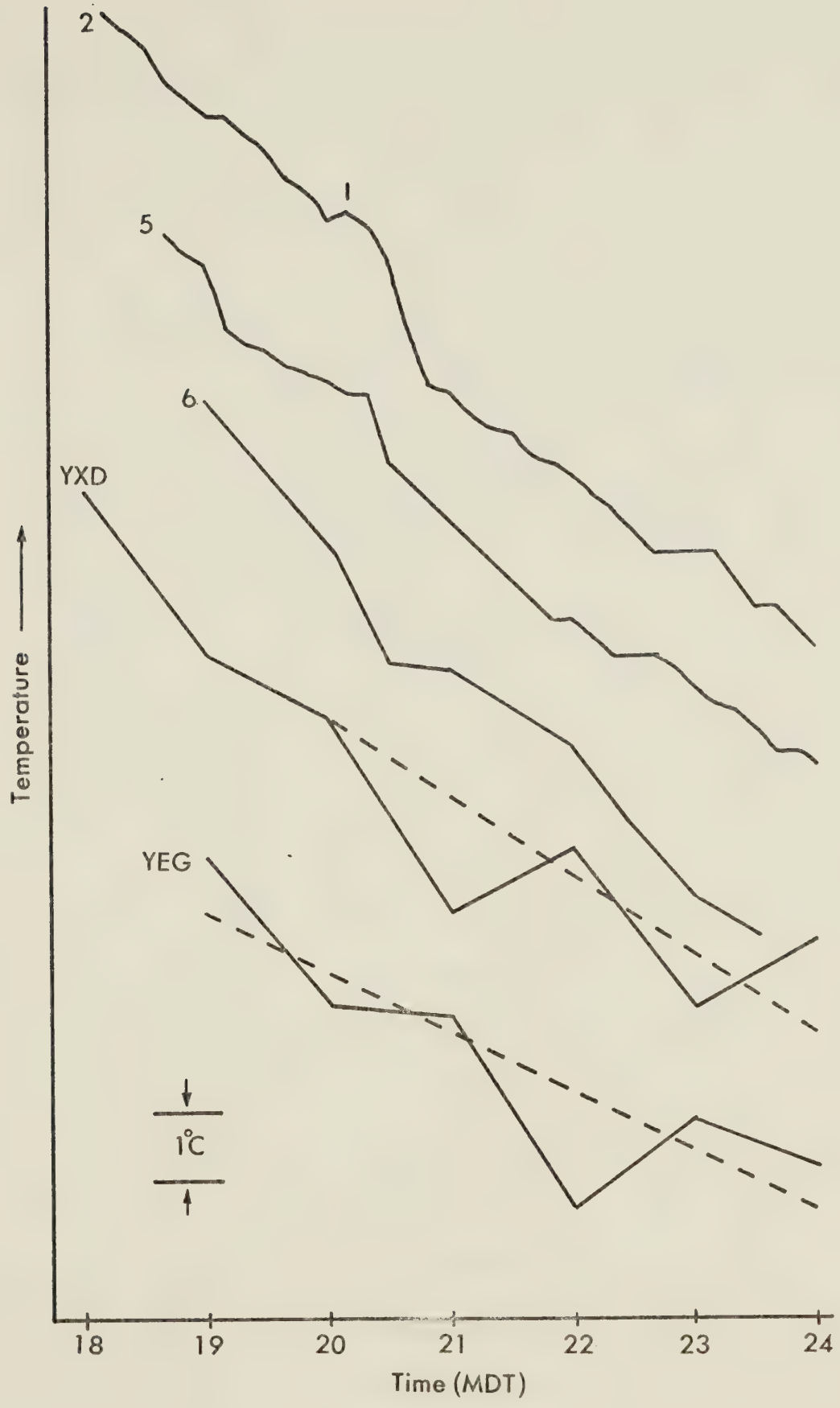

Fig. 3.3. Time plot of temperature for river valley stations not used in profile, including YXD and YEG. Numbers at beginning of plot indicate station.

the other stations. Station 2 did show one period of rapid cooling beginning at 2010, indicated by a tick mark. This time is in agreement with the beginning of the onset of the initial inversion shown at station 4c which was close to the height of station 2. The absence of further rapid decreases in temperature is probably due to the formation of a downslope wind, isolating station 2 from direct interaction with the valley air. The absence of any such initial temperature drop at station 5 is surprising until the actual temperatures are studied (Table 3.2). The temperatures at station 5 were lower than those at any other river valley station and were comparable with those at the rural station YEG. The air temperatures above the rim of the valley at station 1 were comparable to those at the urban station YXD as expected. The north slope and river station (2 and 3) temperatures were midway between urban and rural values. An explanation for the lower temperatures recorded at station 5 may be discerned by studying the change of temperature with time from Experiment 1 (Fig. 3.4). As can be seen, the temperatures at both stations were comparable at 1645, but station 5 began to cool earlier than station 1. When station 1 began to cool at about 2000, the rate of cooling at station 5 was similar and the temperatures at station 5 remained lower than those at station 1. The early cooling of station 5 is consistent with the early shading of the north-facing slope from the sun. This phenomenon was also observed during Experiments 2 and 3 in varying

Table 3.2. Comparison of temperatures (°C) at main river valley stations with the urban airport (YXD) and the rural airport (YEG).

	Station						
Time	1	2	3	5	6	YXD	YEG
1830	8.7	8.4	8.2	--	--		
1900	7.8	7.4	7.4	4.2	8.3	6.6	1.7
1930	7.2	6.9	6.9	3.0	7.3		
2000	6.9	5.9	5.0	2.9	6.2	5.7	-.4
2030	6.2	5.3	3.4	1.4	4.5		
2100	5.2	3.4	2.9	0.5	4.4	2.9	-.6
2130	4.7	2.8	1.9	-.3	3.9		
2200	3.7	2.2	1.6	-.9	3.3	3.8	-3.4
2230	3.2	1.4	1.1	-1.4	2.2		
2300	3.1	1.1	-.4	-1.9	1.1	1.5	-2.1
2330	2.8	-.3	-.6	-2.5	0.6		
2400	2.2	-.3	-.9	-3.0	--	2.5	-2.8

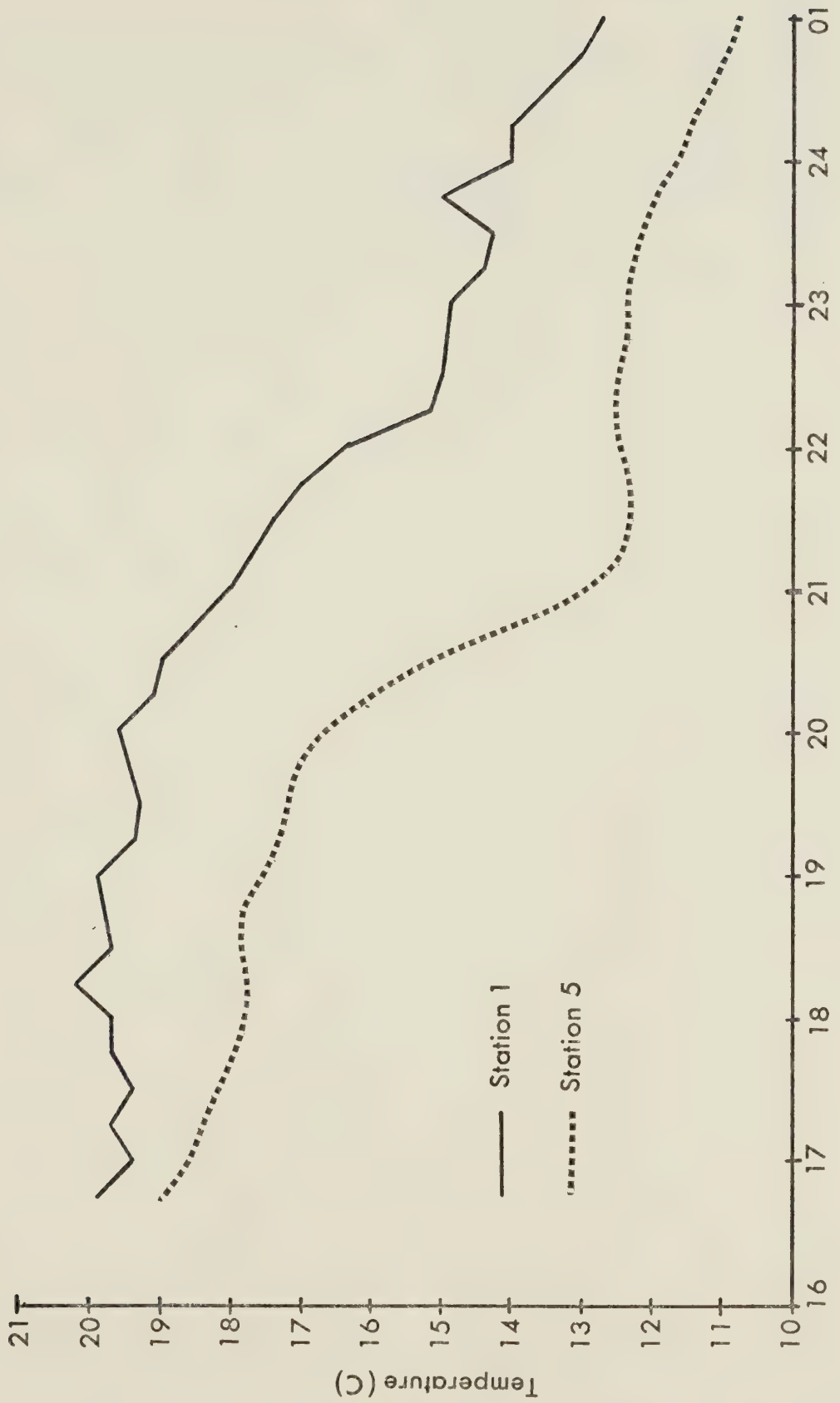

Fig. 3.4. Temperatures for stations 1 and 5 from Experiment 1, July 13-14, 1977.

degrees. Since this difference in temperatures appears to be common on clear evenings it suggests that an east-west segment of the valley is asymmetric in temperature and that little interchange of air occurs between the two sides of the valley, at least near the surface. This casts doubt on the existence of any type of double-vortex closed circulation within such segments of the valley.

CHAPTER 4

RESULTS OF WIND MEASUREMENTS

4.1 Wind Above the River Valley

Wind speed at station 1, representing the above-valley flow, was measured by a three-cup anemometer and the output was recorded on a Rustrak chart recorder. As this chart recorder marks pressure sensitive paper with a striker bar, the recording consists of a series of dots. The density of the dots is too high to enable resolution of the time sequence of successive individual dots, although the trend was obvious. To extract the data, an averaging procedure was adopted, wherein the chart recording was divided into sections and the average value of the trace abstracted by visual observation. This procedure was tested for accuracy by abstracting values by the visual method, then averaging the same data where the value of every point was determined. Errors were found to be less than 10 percent in all cases and less than 5 percent for most cases. The wind speed recording of station 1 was divided into two-minute periods by this method.

The stall speed of the cup anomometer used was 1.5 m s^{-1}. For a wind speed of less than 1.5 m s^{-1}, the indicated wind speed will be zero. Where the wind speed is below the stall speed for only part of the time, the average

value abstracted from the chart will be a measure of the percentage of time the wind speed was above 1.5 m s^{-1}. Where the wind speed remained above the stall speed, the indicated average speed will be correct.

As expected, the wind speed decreased with time and became light as the inversion formed by 2100 (Fig. 4.1) at station 1. The wind direction was from the SE for most of the time, except for the period from 2030 to 2230, when the wind direction became unsteady, backed to WNW for 35 minutes, then veered back to SE. At the same time the wind speed dropped to low values while the wind was unsteady and picked up once the wind had established itself from a given direction. To see if this behavior was truly that of the mean wind, the wind directions from YXD were plotted, and the agreement was generally good considering the distance between the stations and considering that the winds at YXD are measured at the standard 10 m height above ground. Except for the directional shift to WNW at 2200, the mean difference in direction was 20 degrees with a standard deviation of 12 degrees. At 2200 the difference was 90 degrees, indicating that this change in direction must have been related to the river valley and not to the prevailing flow. If the inversion, initiated in the river valley, is assumed to reach above the level of the rim of the valley, the time of arrival would be about 2050, which is the time at which the wind at station 1 began to back to WNW, indicating that the increase in wind speed and the

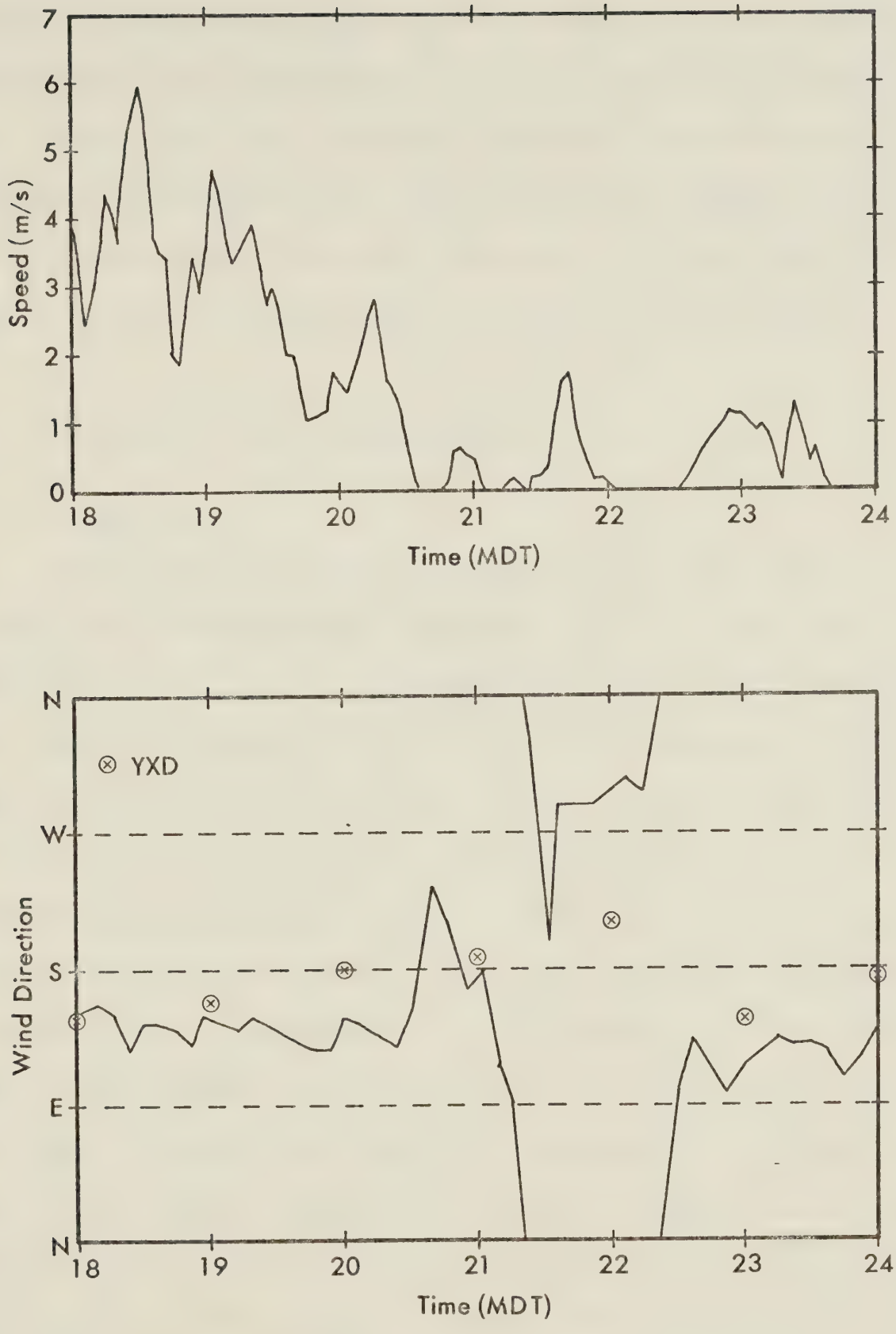

Fig. 4.1. Prevailing wind direction and speed measured at station 1. Wind direction for municipal airport (YXD) plotted for comparison.

change in direction experienced at station 1 were related to the inversion propagating to this level. The temperature at station 1 did show an increase in the rate of temperature decrease, but this was not any larger than the rate of temperature decrease observed at other times and cannot be used to confirm the arrival of the inversion.

4.2 Winds Within the River Valley

4.2.1 Station 3

Wind measurements at station 3 were taken with a three-axis Gill propeller anemometer and two cup anemometers for wind profile measurements. Data were abstracted from chart recordings of the propeller anemometers by the same method that was used for station 1, with averaging times of 1.0 to 1.2 minutes. The horizontally-positioned propellers were aligned along the valley axis (W to E) and across the valley (N to S). The wind speed and direction were obtained by assuming a cosine response for the propellers and summing the individual results vectorially. The actual response of the Gill anemometers has been shown not to be a cosine (Drinkrow, 1972), but the error in this assumption is about 1 percent and is considered small when compared to other sources of error. The chart speeds were not constant over the length of the experiment, so to equate the two components, the chart speed was assumed to be constant between hourly time marks, and values of speed

were interpolated to the same time intervals of 1.2 minutes. The time series was then low-pass filtered to remove the high frequency components of the wind (periods of less than 2.4 minutes), since these components are questionable due to the data extraction method and would not aid in the analysis. The trend of the time series was obtained by low-pass filtering over a one-hour time interval using a Bartlett filter (see Section 4.3.2 for discussion).

Wind profile measurements were made at 1.4 m and 2.6 m levels, with counting cup anemometers over periods of one hour. The average wind speed measured by these anemometers was found not to agree with the one-hour averages obtained from the propeller anemometers, in that the cup speeds were significantly higher for low wind speeds. This effect is probably due to the wind speed being too close to the stall speed of the cups and to the resultant non-linearities. This means that, while the shape of the profile obtained with the cups will be good, the measured wind speeds cannot be equated to other sensors if the wind speed drops below the cup stall speed for a portion of the time. When the average wind speeds were greater than 1.0 m s^{-1} the profiles, including the propeller anemometer data, were reasonable (Fig. 4.2). After 1900, when the average speeds were below 1 m s^{-1}, the inclusion of the propeller data is dubious. The cup anemometers do, however, indicate that the wind speed increased with height before 2000 and became almost constant with height thereafter.

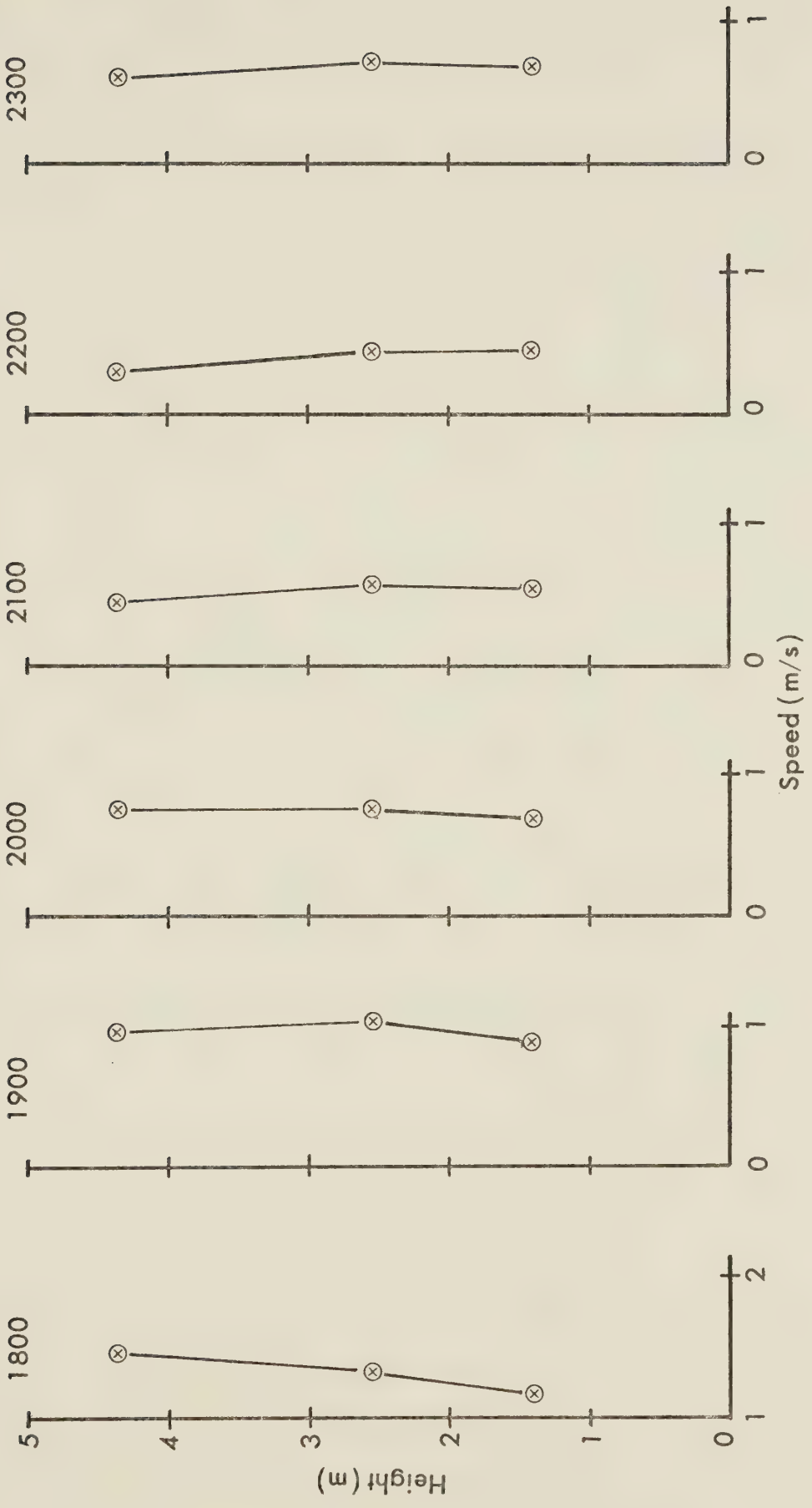

Fig. 4.2. One-hour wind profile averages at station 3 beginning at the time indicated.

The wind speed at station 3 dropped to low values at 2200, then picked up to a constant speed of about 0.6 m s^{-1} after 2300 (Fig. 4.3). This is surprising, as the wind speed would be expected to become very low with a well-developed inversion in the valley, but an examination of wind direction data indicates the reason for this (Fig. 4.4). Before the formation of the inversion after 1940, the wind was blowing from the east and it began to veer at 1940 to become westerly by 2040. The period 1940 to 2040 was the time required for the inversion to completely fill the river valley. Thereafter the wind was always westerly. The westerly wind in the valley within the inversion layer was in accord with the change of wind direction to westerly at station 1. This suggests the idea that the inversion propagated above the rim of the valley.

There are several possible explanations for the switch to a westerly wind. The river runs at a considerable velocity in an easterly direction and frictional drag might pull the air with it. However westerly winds in the river valley with a southerly prevailing wind have been observed with the river frozen over. The slope of the river valley may also cause a drainage effect, but the slope of the river is only 0.9 m/km and this does not seem to be a reasonable explanation for the rapid shift in direction in synchronization with the formation of the inversion. The most plausible theory is tied to the geographical alignment of the North Saskatchewan River Valley

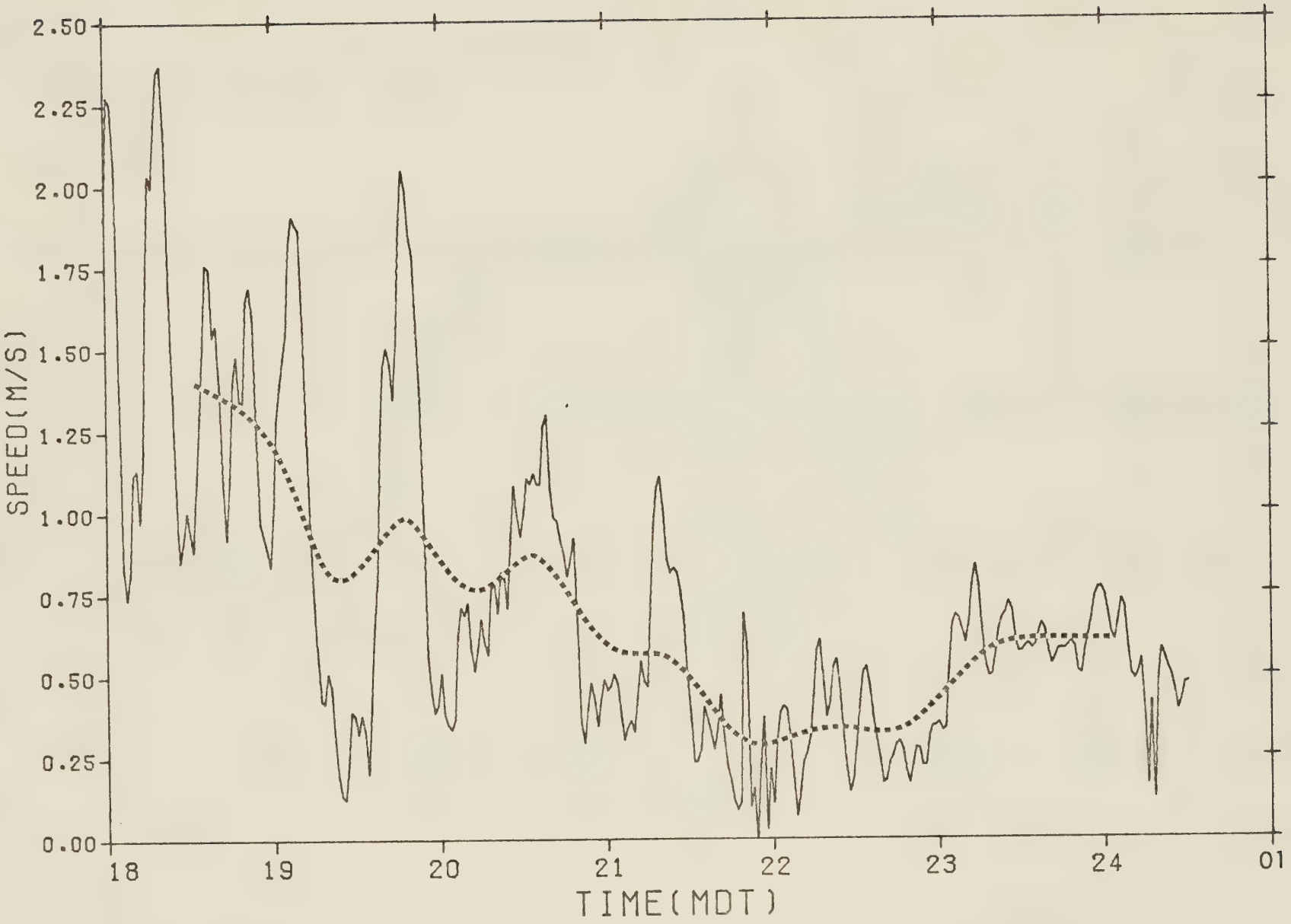

Fig. 4.3. Wind speed at station 3. Dotted line indicates trend. Series filtered with 5-point Bartlett filter.

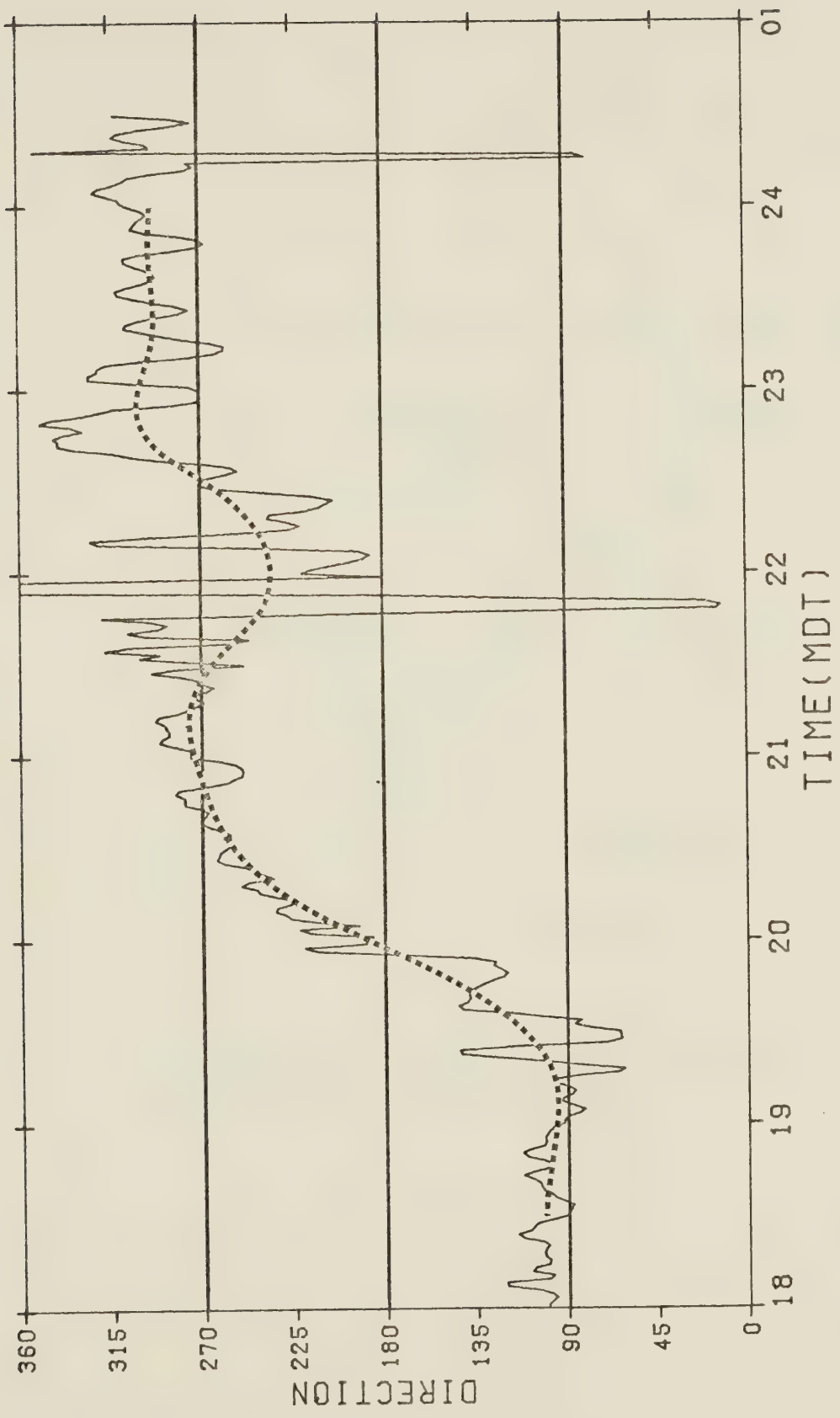

Fig. 4.4. Wind direction at station 3. Dotted line indicates trend. Series filtered with 5-point Bartlett filter.

system. The river is generally aligned SW to NE and consists of a series of meanders that are generally aligned N to S and W to E (Fig. 2.1). This can be represented schematically (Fig. 4.5). Although once the inversion is

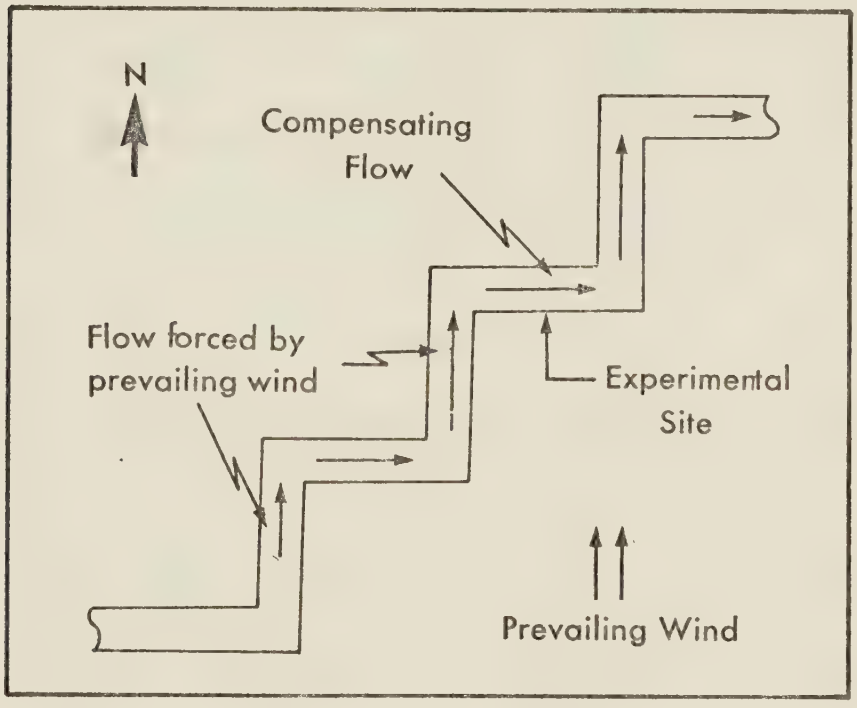

Fig. 4.5. Schematic of North Saskatchewan River Valley system showing possible cause of westerly winds at experimental site.

established, the valley air is expected to be isolated from the prevailing wind, if the prevailing wind blows parallel to the valley axis, the air in the valley will tend to move with the wind and there will be an increase in mass in the leeward end of the valley and a decrease in mass in the windward end. Since the river valley is arranged stair-

case fashion, a southerly wind will move the air in the N-S aligned segments of the valley northward, and the resulting pressure gradient across the E-W segments of the valley would establish a westerly flow within those segments. This could happen rapidly and could account for the rapid directional change in the valley wind. This theory, however, appears to be only part of the explanation, for a westerly wind in the valley in winter when the river is frozen has been observed with calm prevailing winds as evidenced by vertically-rising plumes from sources within the city.

Vertical velocity was also measured at station 3 and recorded on a Rustrak recorder. As mentioned previously, it was not possible to distinguish the time sequence of successive dots and, in the case of vertical velocity, when the signal switches rapidly from positive (upflow) to negative (downflow), the previously-used averaging procedure will not give any significant information about vertical velocity. In order to derive statistical information, the values of each recorder trace were abstracted for a given time period. In this case a period of five minutes was chosen. Four such periods were abstracted and the means and variances were calculated. The variance of the vertical velocity with time is shown in Fig. 4.6, the final reading being an estimate, as the signal levels were too low to enable the value of individual dots to be read. After this time the signal was below the noise level

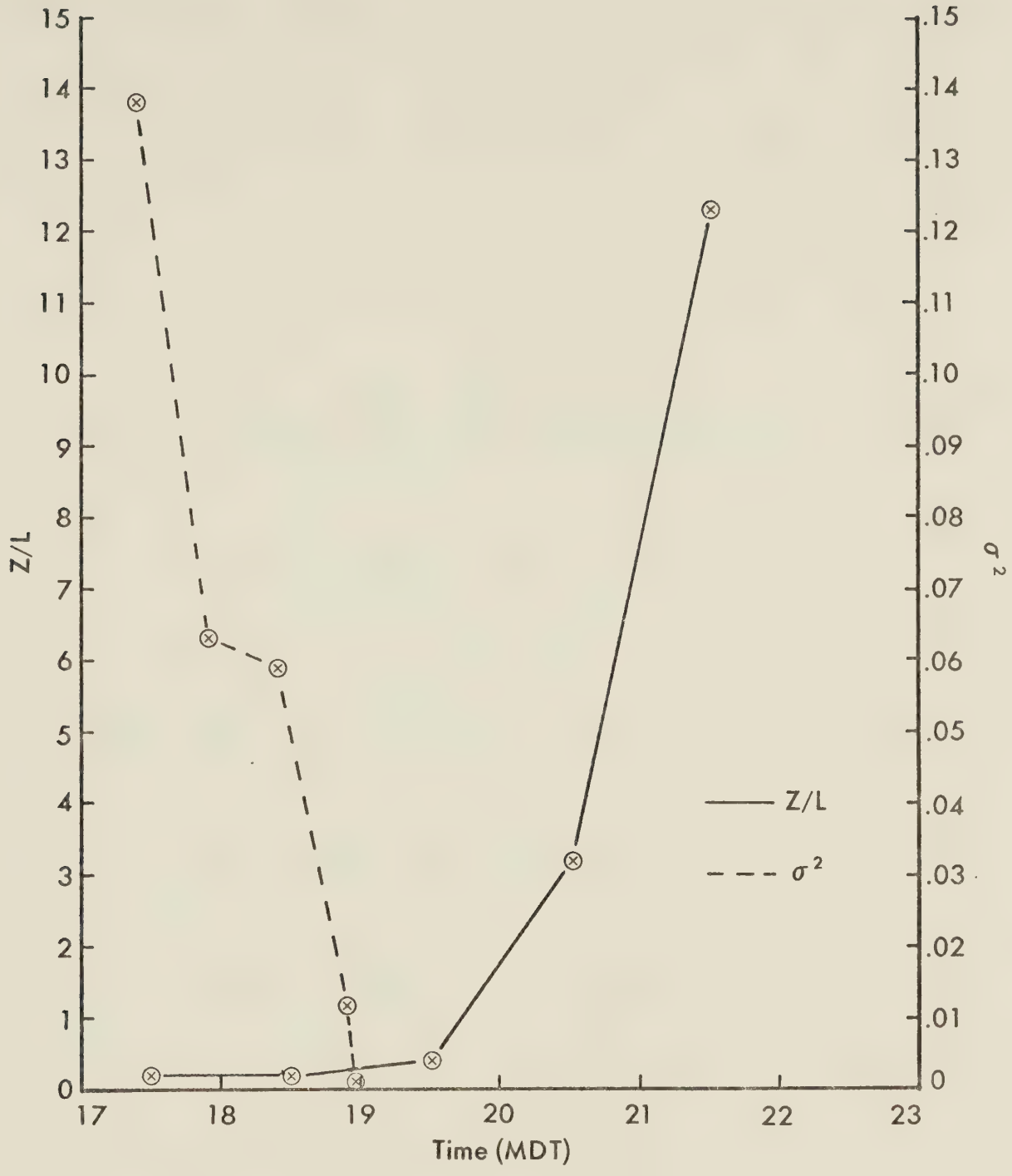

Fig. 4.6. Stability (Z/L) and variance of vertical velocity (σ^2) at station 3.

of the recorder, indicating no movement of the anemometer. Measurable vertical velocity activity did not end at 1900, but the activity cannot be described in a statistical way, as later activity occurred in short bursts, as if stress built up, then released. The first measurable activity occurred at 1940, with a brief upward burst of 0.4 m s^{-1}. Four more bursts of upward motion occurred in the next ten minutes, then at 2000 activity occurred for five minutes with peak velocities of 0.9 m s^{-1}. After this there was no activity until 2143, when a very brief burst of 0.2 m s^{-1} occurred for 20 seconds. Vertical velocities were observed again from 2200 to 2208 with peak velocities of 0.3 m s^{-1} and at 2215 with peak velocities of 0.3 m s^{-1}. After this time no activity was recorded.

As a check on the consistency of the data, stability was determined from the available information at station 3 and from the lowest level of the temperature profile 4d. The stability parameter is Z/L where L is the Monin-Obukhov length. As L could not be determined due to the unavailability of surface heat flux measurements, the assumption was made that Z/L was equal to the gradient Richardson number, R_i (Panofsky, 1973). This assumption may be questionable in stable conditions, but will indicate the trend in stability. Thus we have

$$R_i = \frac{g}{T}\left[\frac{\partial\theta/\partial Z}{(\partial U/\partial Z)^2}\right]$$

where g = acceleration of gravity

θ = potential temperature

T = mean temperature

and where the partial derivatives were evaluated for a logarithmic profile using (Paulson, 1970)

$$\frac{\partial F}{\partial Z} \cong \frac{F_2 - F_1}{(Z_1 Z_2)^{1/2}} \ln(Z_2/Z_1)$$

where F is, for example, θ or U and the derivative is determined for the height $(Z_1 Z_2)^{1/2}$. The wind speeds were taken from the cup anemometers at 1.4 and 2.6 m. Although the values measured by the wind profile system are questionable, the change in velocity with height will be valid, as the errors in the measurements are common and should cancel. The temperatures were evaluated from the thermograph temperature at station 3 and the thermocouple temperature from 4d. The change of temperature with height between these two levels was assumed constant. As the stability is sensitive to temperature, the temperatures were averaged one an hour to eliminate random errors and to match the one-hour wind speed averages from the anemometers. Fig. 4.6 shows that, consistent with the time of onset of the inversion at 1940 MDT, the stability increased rapidly.

4.2.2 Station 2

The upslope (north) and downslope (south) component of the wind at station 2 was measured with a propeller anemometer, but the cross-slope component was not measured due to equipment problems. The data were abstracted and filtered and the trend calculated by the same process as that used at station 3. The averaging period was 1.2 minutes and the trend was calculated over one hour. As an earlier study by Klassen (1962) indicated that the drainage flow was weak and shallow, cup anemometers were arranged to measure the wind profile at 1, 2 and 3 m. The cup anemometers used were of the same type as those used at station 3 and the earlier discussion of their limitations and errors pertains as well to the profile measurements at station 2.

In the early period of the evening the wind was blowing upslope, either in response to the mean flow or indicating that a daytime type of valley circulation was still occurring (Fig. 4.7). As the effect of nocturnal cooling made itself felt, the wind at station 2 decreased in intensity and at 1940 began blowing downslope, indicating the establishment of a drainage flow. At 2000 the wind again blew upslope continuing until 2030, when it once again began blowing downslope and established a drainage flow, except for a few brief periods from 2230 to 2300, when the temperature remained constant. Although no wind direction measurements were available, the flow was con-

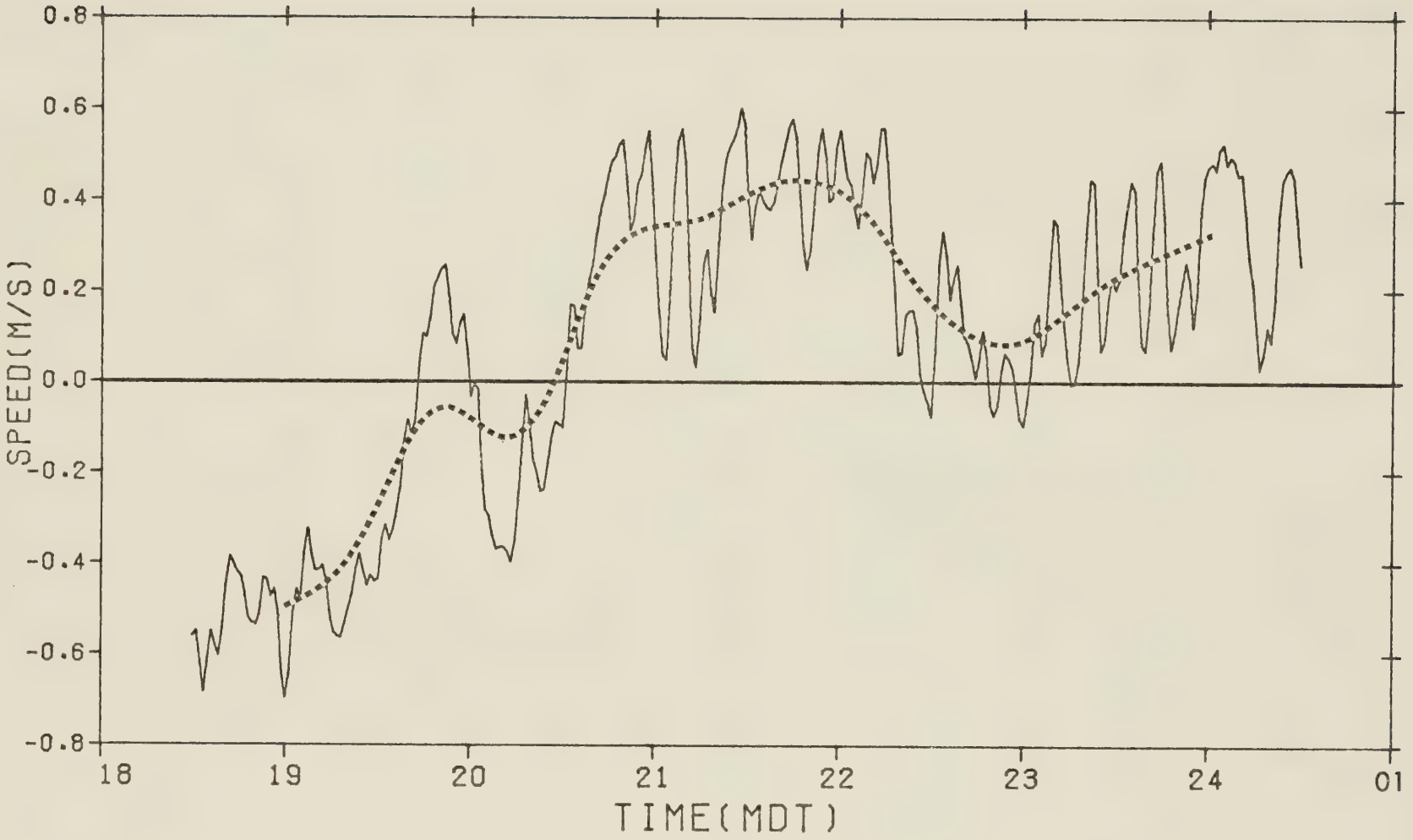

Fig. 4.7. Downslope wind component at station 2. Positive values indicate downslope flow and dotted line the trend. Series filtered with a 5-point Bartlett filter.

firmed as downslope by the station operator for the latter part of the experiment. From the temperature record, the inversion was seen to arrive at station 2 about 2010, although the maximum rate of cooling was not experienced until 2030, when the wind at station 2 became downslope. The timing of the arrival of the inversion and the activity of the wind, suggest that the upslope wind that occurred after the initial downslope regime was established and the inversion were connected. The most likely explanation for this is that the inversion layer acts as a 'floor' to the penetration of the prevailing wind so, as the inversion layer thickens, the mean wind flow will be constrained to a shallower depth in the valley and thus affect the slope winds. Without a measure of the cross-slope wind component, however, it is not possible to determine if the flow is SE (the prevailing flow) or W (the channeling effect which resulted in the westerly winds at station 3).

The wind profiles reflect the normal increase in wind speed with height, until the period 2030-2100 MDT, and are close to the theoretical logarithmic shape expected in the constant-flux layer (Fig. 4.8). From the period 2030-2100 onwards, after the drainage wind had established itself, the profiles indicate a constant wind speed with height, showing that the drainage wind, although light, was much deeper than expected. Observation of a steam exhaust plume from the Glenora Club did not show evidence of the down-slope flow at 2100, but by 2350 the plume was observed to

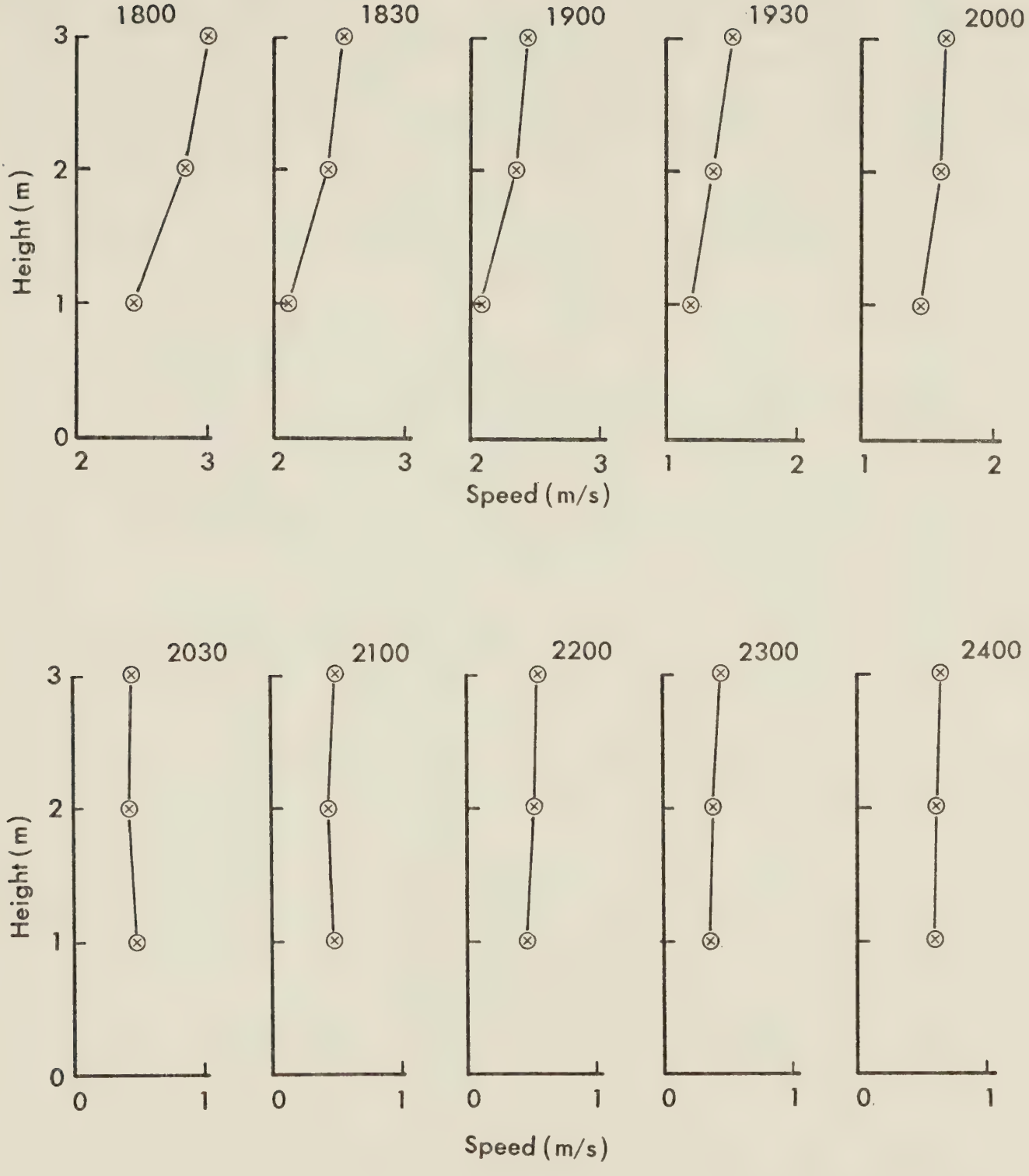

Fig. 4.8. Wind profiles from 1800 to 2400 MDT at station 2. Profiles are half-hour averages beginning at the time indicated at top of graph.

drifting southward, indicating that the drainage flow had extended in depth, on the river flood plain, to the top of the building at 15 m. Evidence that the drainage flow reached the height of the propellor anemometer array at station 3 can be seen from the cross-valley wind component, which was consistently from the north after 2230.

4.2.3 Station 5

The upslope (south) and downslope (north) component of the wind was measured with a propeller anemometer and the wind direction with a vane. The data were abstracted and filtered, and the trend was calculated with the same parameters that were used for station 2. A plot of wind direction was not produced as the wind was downslope from 1830, when measurement began, to 0100, the end of the experiment (Fig. 4.9), and the measured wind direction was 180 degrees $\pm$ 15 degrees. As noted in Chapter 3, the temperatures measured at station 5 were lower than those at any other station because cooling began first at this station. It was also noticed that the temperatures implied a different regime at station 5, and this is reinforced by the wind measurements. The downslope wind with no significant time variation in the trend implies a well-developed drainage flow at 1830, with stable conditions. This again suggests that conditions on the south slope are different and isolated from conditions elsewhere.

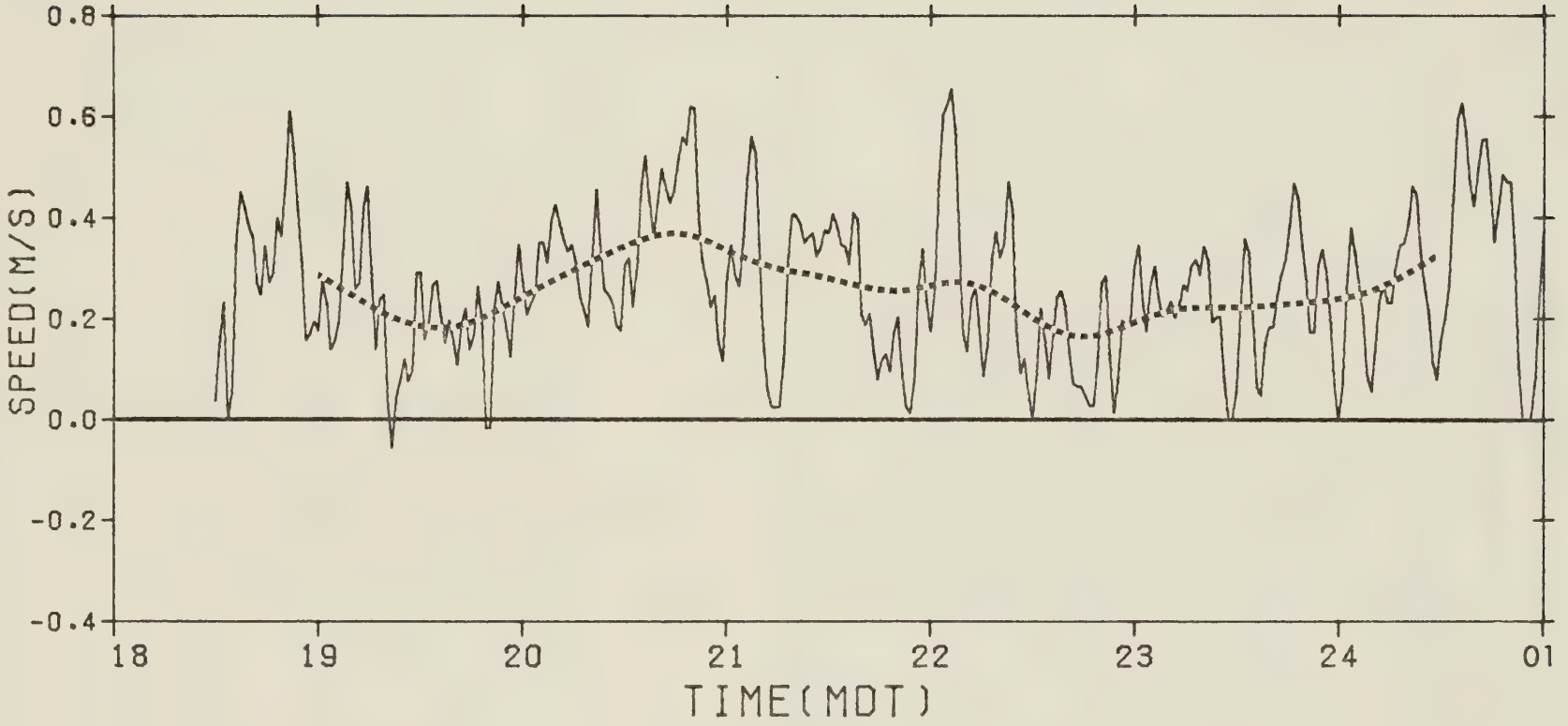

Fig. 4.9. Downslope wind component at station 5. Positive values are downslope wind and trend is indicated by dotted line. Series filtered with a 5-point Bartlett filter.

4.3 Spectral Analysis of Winds

During study of the wind speeds, there appeared to be a regular variation in speed, especially at the river valley slope stations. A simple correlation between station 2 wind and the cross-valley wind component of station 3 resulted in a correlation of 0.95, which suggested a periodicity since any random variation would be smoothed by the distance between stations. However, a periodicity does not seem probable as there is no apparent mechanism to result in such periodicities. The simple regression used is not suitable for the purpose of determining if the correlations reflect real periodicities as sensitivity is low. As an alternative the wind speed measurements were subjected to spectral analysis.

4.3.1 The Spectral Program

The spectral analysis program used was devised by Lachapelle (1977) and uses the Fast Fourier Transform (FFT) as the basis for the modified periodogram method of analysis. The data were first preconditioned by the program as follows:

1. The mean, variance and standard deviation were calculated.
2. The mean was removed.
3. Zeroes were added to the data set to reach a size of 2^n.

4. The data were standardized by using the relationship

$$Y_i = (X_i - \bar{X})/S$$

where $\bar{X}$ is the mean, and S is the standard deviation.

The standardized data were then passed to the FFT programs and the results made available in printed and computer-plotted form. Provision was made for smoothing the periodogram using a Daniell window. This is recommended by Kanasewich (1975), as it reduces the variance of the periodogram and produces a spectral estimate that will more likely be replicated if the experiment is repeated.

4.3.2 Filtering

Although the wind data were smoothed by the method of abstraction from the recorder charts, there was still a considerable amount of high frequency energy in the data which was of questionable value, as it added noise to the frequencies of interest. To remove these high frequencies, the data were filtered with a low-pass filter and as a result the characteristics of the filter used must be known to assess the effect on the data. The frequency response of the filter is the ratio of the amplitude of a wave of a given frequency in the series after filtering to the original amplitude before smoothing and this frequency

response is a function of frequency. The response function of a filter is given by

$$R(f) = \int_{-\infty}^{\infty} W(t) \exp(-2\pi i f t) dt \qquad (4.1)$$

where $f = \frac{1}{T}$, T = smoothing interval

$W(t)$ = weight function

This equation is the inverse Fourier transform of $W(t)$ and therefore the inverse Fourier transform of the filtering function is the filter's response function. The absolute value of $R(f)$ is

$$|R(f)| = [(\mathrm{Re}\{R(f)\})^2 + (\mathrm{Im}\{R(f)\})^2]^{1/2} \qquad (4.2)$$

and the phase angle

$$\phi = \tan^{-1}[\mathrm{Im}\{R(f)\}/\mathrm{Re}\{R(f)\}] \qquad (4.3)$$

The discrete form of the filter is

$$R(f) = \sum_{k=-n}^{m} W_k \exp(i2\pi f k) \qquad (4.4)$$

Since it is desired that the filter not phase shift waves

at any frequency, Im{R(f)} must be required to be zero. This can be accomplished by requiring W(t) to be even (namely, W(-t) = W(t) or in the discrete case $W_{-k} = W_k$). If W(t) is even, the filter is called symmetric and the response function is

$$R(f) = \int_{-\infty}^{\infty} W(t) \cos(2\pi ft)dt$$

$$= 2 \int_{0}^{\infty} W(t) \cos(2\pi ft)dt \qquad (4.5)$$

or for discrete filtering having 2m + 1 weights

$$R(f) = \sum_{k=-m}^{m} W_k \cos(2\pi fk)$$

$$= W_0 + 2 \sum_{k=1}^{m} W_k \cos(2\pi fk) \qquad (4.6)$$

Taking the simplest filter, an equally-weighted running mean or box car filter, where every weight is equal, the response function is computed from equation (4.5) using

$$W(t) = \begin{cases} 1/T & |t| \leq T/2 \\ 0 & |t| > T/2 \end{cases}$$

Equation (4.5) gives

$$R(f) = 2 \int_0^{T/2} \frac{1}{T} \cos(2\pi ft)dt$$

$$= \frac{\sin(\pi ft)}{\pi ft} \qquad (4.7)$$

The response function is shown in Fig. 4.10. The meaning of the negative response in Fig. 4.10 is that, as well as being changed in amplitude, the waves are reversed in polarity, that is, the phase is shifted 180 degrees, so that maxima are changed to minima and vice versa. This characteristic, plus the large value of the response variation above the frequency of the first zero pole in the response (side-lobes), makes this type of filter undesirable.

The Bartlett filter is defined as

$$W(t) = \begin{cases} 1 - |t|/T/2 & |t| \leq T/2 \\ 0 & |t| > T/2 \end{cases} \qquad (4.8)$$

and the response function is

$$R(f) = 2 \int_0^{T/2} \left(1 - \frac{2t}{T}\right) \cos(2\pi ft)dt$$

$$= \frac{T}{2} \left[\frac{\sin \frac{\pi ft}{2}}{\frac{\pi ft}{2}} \right]^2 \qquad (4.9)$$

As can be seen (Fig. 4.11), the side-lobes are small, the first being 4.5 percent of unit response and all side-lobes are positive, indicating no phase reversal. This response is much more desirable in that it maintains phase relationships and is reasonably good at supressing frequencies above the first response pole. The Bartlett filter was chosen as the operating low-pass filter with the first zero pole set equal to the Nyquist frequency.

In addition to the high frequencies, the trend must also be removed from the data, or the power contained in the trend will load the low frequency end of the spectrum and cascade or leak through to higher frequencies of the spectral estimate and invalidate the results of the power spectrum analysis at many frequencies. A high-pass filter was used for this purpose. The high-pass filter was synthesized from the low-pass Bartlett filter by first deriving the low frequency trend from the series, then subtracting this trend from the original time series. The resulting response function will be the inverse of that for the low-pass filter.

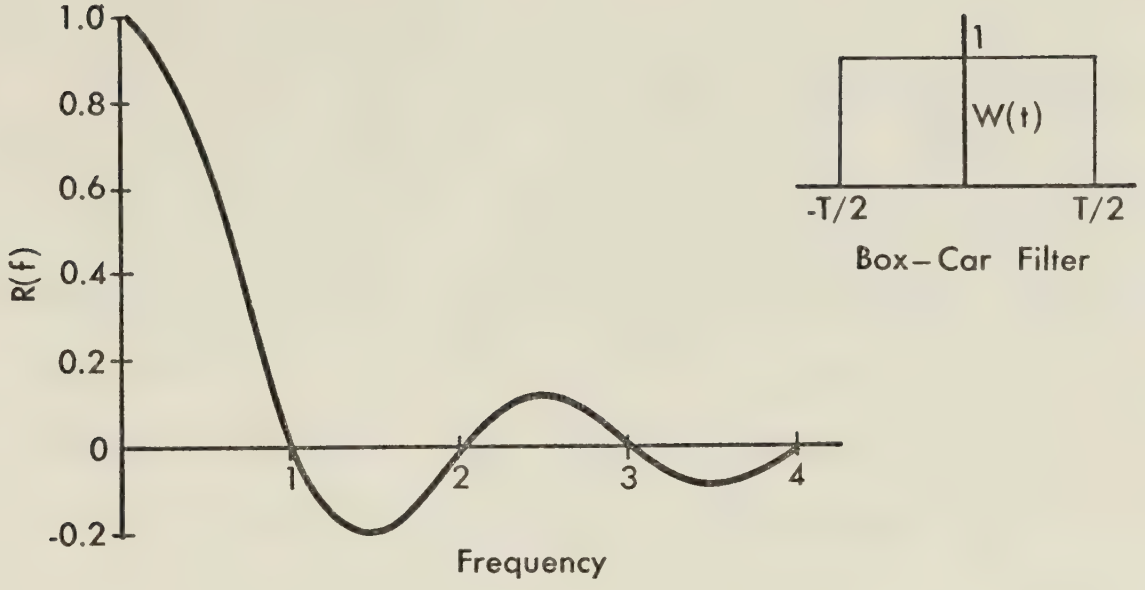

Fig. 4.10. Box-car filter and its response function.

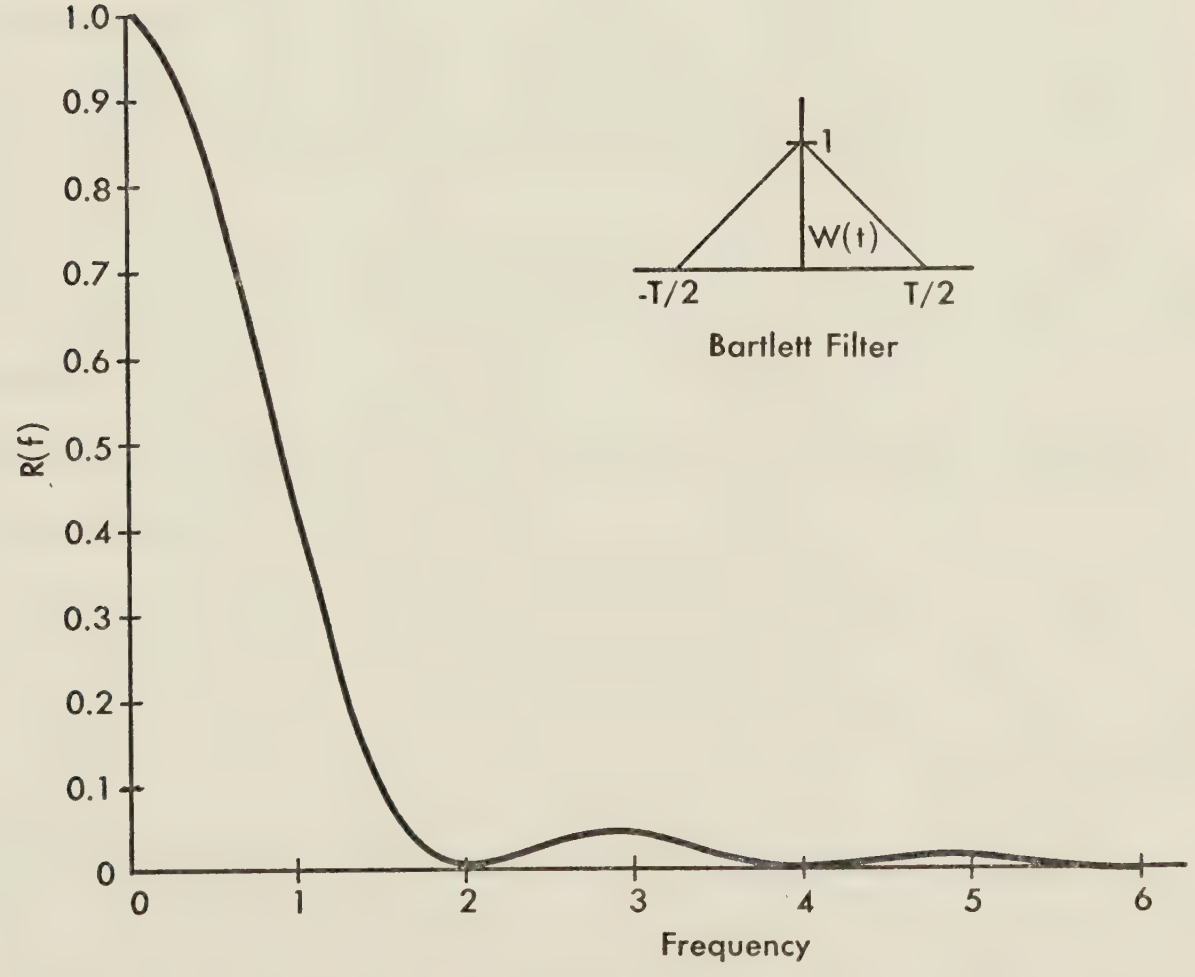

Fig. 4.11. Bartlett filter and its response function.

4.3.3 Confidence Limits

To evaluate the time series, the significance level of the spectral peaks must be determined. Generally, confidence limits are generated by assuming a randomly-varying time series usually called white noise, that has a constant power per unit frequency. The test statistic is then the ratio of the sample variance of the line to the variance of the white noise. In many meteorological applications, the use of a white noise source is not possible. One of the characteristics of many meteorological spectra is a general suppression of relative variance at high frequencies as compared to an even distribution of variance across the spectrum expected from a white noise source. This characteristic is caused by the appreciable auto-correlation found in meteorological data and has been called red noise (Gilman et al., 1963). The red noise spectrum may be derived by considering a first-order linear Markov process, where a discrete time series depends only on its own immediate past value plus a random component. This may be represented by

$$X_n = \rho X_{n-1} + Y_n \tag{4.10}$$

where $E(\overline{Y}_n)$, the expected value of Y_n equals zero

$$\overline{Y}_n^2 = \sigma^2$$

$\rho = \rho(1)$, the population value of the lag 1 autocorrelation

It has been shown by Gilman et al. (1963), that the estimate of spectral density as a ratio of red noise to white noise can be expressed in the form

$$\frac{\rho^2(\omega)}{\rho^2/m} = \frac{1 - \rho^2}{1 - 2\rho \cos \omega + \rho^2} \tag{4.11}$$

where ω is the frequency

$\sigma^2(\omega)$ is the variance of the red noise spectrum at frequency ω

σ^2/m is the variance of white noise per line

m is the number of spectral lines

In the spectral program, the spectrum is normalized, so that $\sigma^2 = 1$. For red noise $\rho(t) = \rho(1)^t$ and if the sample has come from a parent population which represents the red noise process, then each sample autocorrelation value should provide the means to estimate ρ, the population lag 1 autocorrelation (Eddy, 1968). Since the values used should be those which are statistically significant and since the lag 3 autocorrelation value of the sample winds was around 0.05, ρ was estimated from the sample by

$$\rho = \left(\frac{R(1)^2 + R(2)}{2}\right)^{1/2} \tag{4.12}$$

where R(L) is the sample autocorrelation of lag L.

The statistic to be tested during the red noise hypothesis is the ratio of the sample variance of the line to the red noise at that same frequency. For n pieces of independent data and m spectral lines, the equivalent number of degrees of freedom for the Chi-square distribution of a spectral line is

$$\nu = \frac{2n - m/2}{m} \tag{4.13}$$

Meteorological data are not independent due to the high autocorrelation, so that the number of degrees of freedom of the data is

$$n' = n\left(\frac{1 - \rho^2}{1 + \rho^2}\right) .$$

Due to the bandpass filtering of the original data, not all spectral lines will follow the red noise model. At those frequencies outside the pass-band of the filters, the spectral lines will contain far fewer degrees of freedom than those inside the pass-band, since the correlation of those frequencies outside the pass-band is much higher due to the filtering action. For simplicity, the assumption was made that all the degrees of freedom contained in the data would go into those spectral lines within the pass-band

where the red noise model was valid. The red noise model fit well in the spectrum of wind speeds from a frequency of 0.02 to 0.24 resulting in an effective number of spectral lines m' = 70 compared to 128 in the complete spectrum (Fig. 4.12).

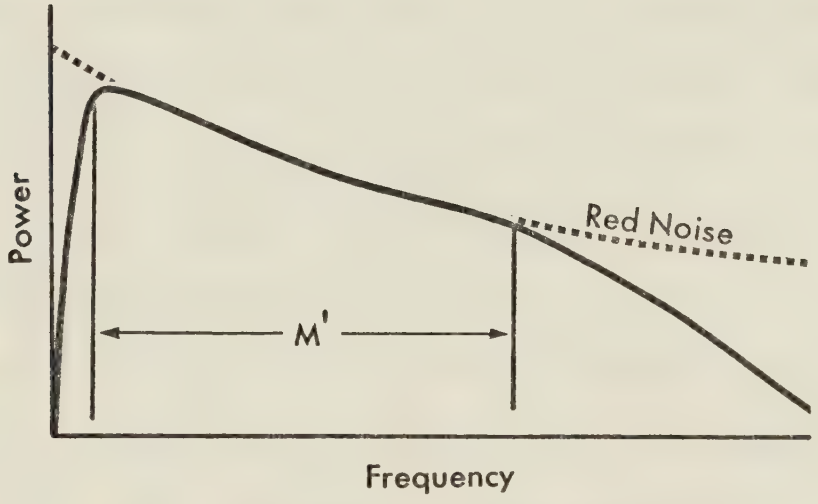

Fig. 4.12. Effect of band-pass filtering on spectrum compared to red noise model.

The filtered spectrum, which is smoothed by a Daniell filter, has the number of independent spectral lines reduced by 1/Md, where Md is the number of points in the Daniell filter (for unsmoothed spectrum Md = 1). The degrees of freedom per spectral line is then

$$\nu = \left(\frac{2n' - m'/2}{m'}\right)Md \qquad (4.15)$$

Confidence intervals were calculated using a Chi-square distribution. The confidence limits were obtained by multiplying the red noise value by $\chi^2_{1-\alpha}/\nu$ and χ^2_{α}/ν for the upper and lower limits, respectively, where α is the probability level selected. Since the degrees of freedom vary between one and two for the unsmoothed spectrum and since the distribution of the Chi-square function varies non-linearly between the values of ν, graphs were plotted of the Chi-square function in order to obtain more accurate estimates of the confidence intervals for the unsmoothed spectrum. The same was done for the confidence intervals of the smoothed spectrum.

The 95 percent and 5 percent confidence levels and the red noise spectrum were drawn on the graphs as shown in Fig. 4.13. All spectral lines exceeding the upper limit were tabulated and the significance levels were calculated. The confidence limits were also drawn on the filtered spectrum and the results compared to the unfiltered spectrum (Fig. 4.14).

4.3.4 Results

Table 4.1 shows the results obtained from the unsmoothed periodogram and lists only the peaks for the probability level $\geq$ 95 percent and for percent variance explained greater than 1 percent, as peaks that explain such a small percentage of the variance would not be of much practical interest. Where there were two peaks to-

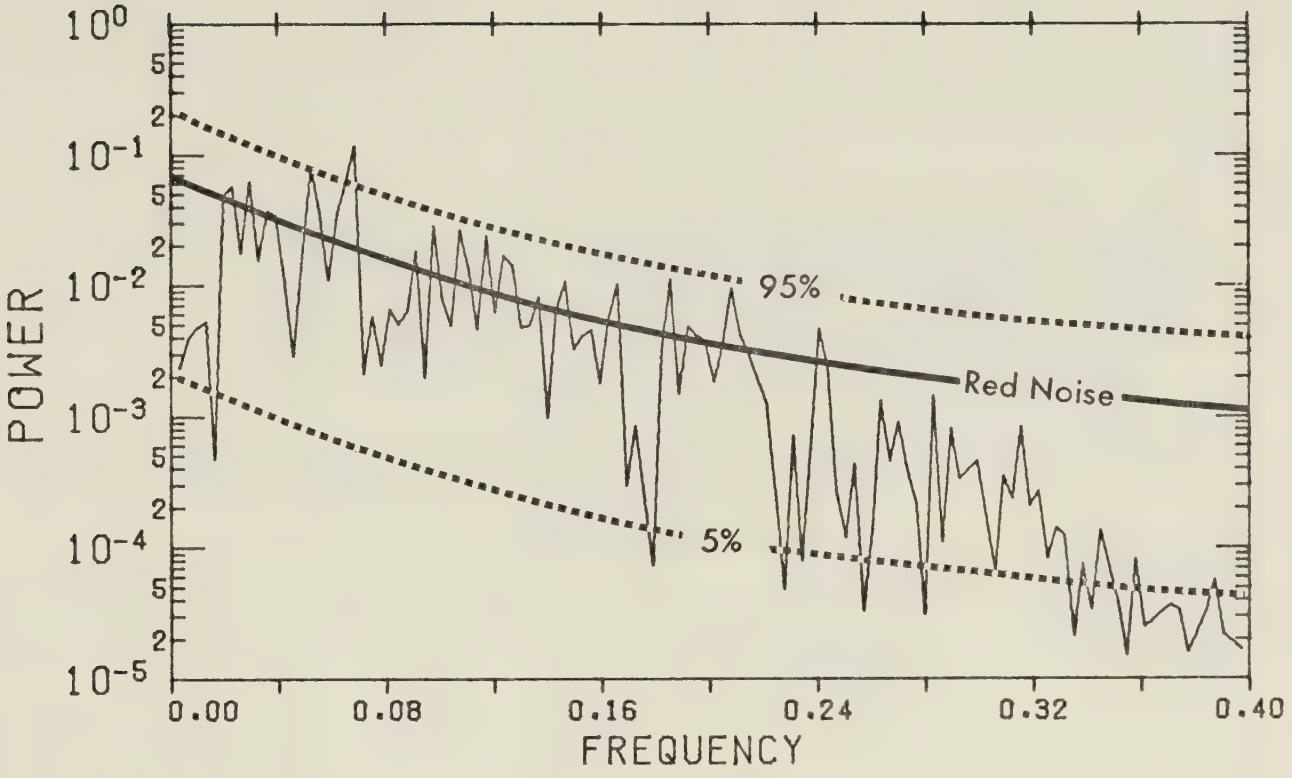

Fig. 4.13. Unsmoothed periodogram analysis of station 5 wind showing red noise spectrum and a 90% confidence interval.

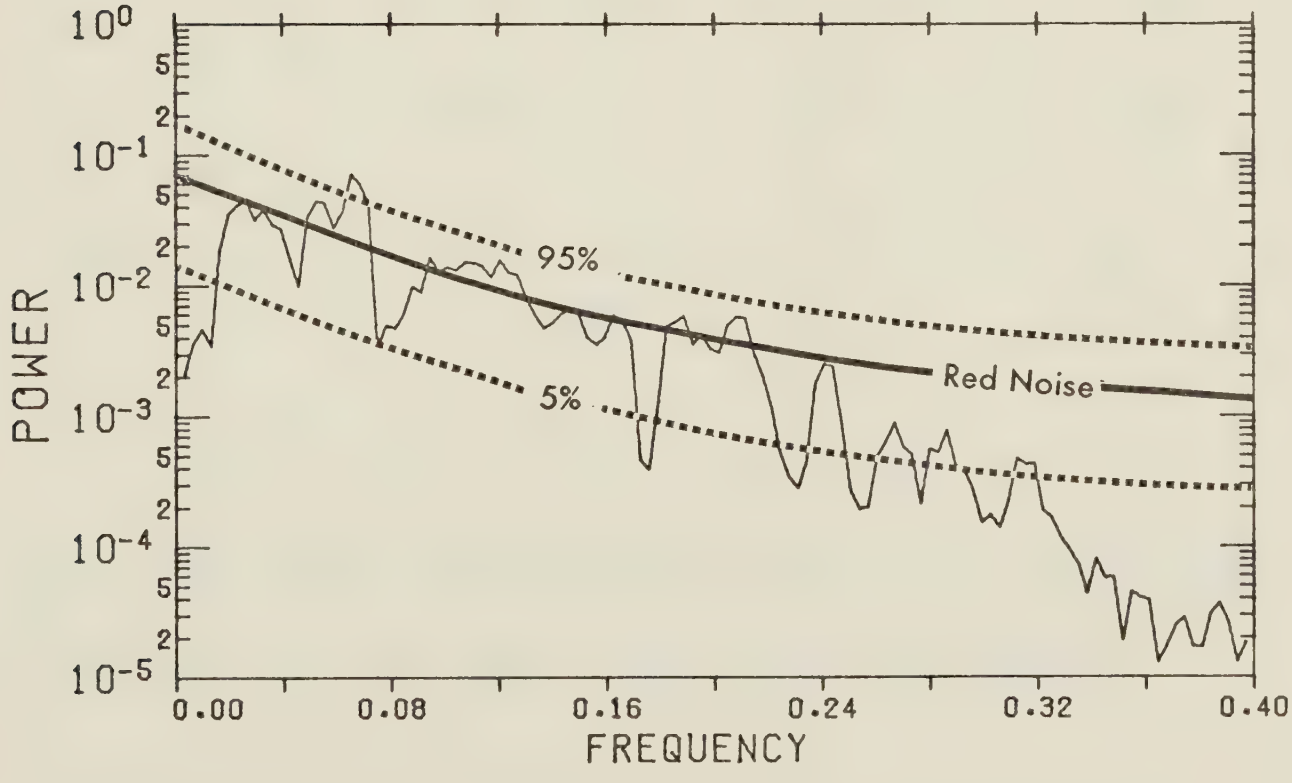

Fig. 4.14. Three point Daniell-filtered periodogram analysis of station 5 wind showing red noise spectrum and a 90% confidence interval.

Table 4.1. Periods (minutes) of significant peaks and significance levels (P %) for station winds from unfiltered periodogram. Cross-valley and along-valley wind components at station 3 are indicated by V and U, respectively.

Station	P(%) 99	97.5	95	% Variance Explained
2			11.0	4.6
		9.6		4.9
	7.9			4.6
		6.0		1.5
3-V			18.1	8.9
			7.7	3.2
3-U			51.2	24.2
		19.2		7.5
5	14.6+			11.6
			19.2	8.0

+ Indicates that the peak exceeded the 99.5% level.

gether near the same probability level, only one was listed as it is probable that adjacent peaks represent variance in the same frequency. With 70 spectral lines 3.5 would be expected to equal or exceed the 95 percent confidence level and, in all cases, this was observed, with 3 or 4 peaks at or above 95 percent. Table 4.2 lists the significant peaks for the 3-point filtered spectrum.

In Table 4.1 station 2 shows four significant peaks, although the peak at six minutes explains little variance. The peak at 7.9 minutes would seem to be the most significant and most likely to represent a real periodicity. However a comparison with Table 4.2 shows that the peak is resolved at 8.1 minutes and has decreased in significance. This indicates that there is little likelihood of periodicities at station 2.

Neither wind component at station 3 shows a peak above 97.5 percent in Table 4.1 and in Table 4.2 little changes except that the peak at 18.1 minutes has moved up from a 95 percent to a 97.5 percent significance level. Thus it is doubtful that a real periodicity exists.

Station 5 shows two peaks in Table 5.1, one at 14.6 minutes explaining 11.6 percent of the variance and significant to better than 99.5 percent. This would appear to reflect a true periodicity, but chance could dictate this result. That the periodicity is real is supported in Table 4.2, where the period appears at 15.4 minutes and the significance level has increased to over 99.9 percent.

Table 4.2. Periods (minutes) of significant peaks and significance levels (P %) for station winds for 3-point Daniell-filtered periodogram. Cross-valley and along-valley wind components at station 3 are indicated by V and U, respectively.

	P(%)			
Station	99	97.5	95	% Variance Explained
2			9.6	2.9
		8.1		2.6
3-V		18.1		6.7
			7.5	2.3
3-U		19.2		5.2
5	15.4+			7.2

+ Indicates that the peak exceeded the 99.9% level.

The actual period was probably 15 minutes. Two questions must be answered. Does this periodicity make physical sense, and is there independent evidence of periodicity? The south slope is heavily wooded, which could act as a friction brake (reducing movement) until the air cooled enough to increase its density and thus its speed, where the increase in speed and the resulting mixing would slow down the cooling and thus slow down the air. As well station 5, unlike station 2, was located at the foot of the slope on a plateau, so that the measurements showed the effect of the entire slope on the drainage wind. There should have been a measurable effect on the temperatures at station 5, resulting in faster cooling during wind speed minima than when the wind speed was a maximum. Unfortunately, the resolution of the thermograph was not sufficient to observe this effect and provide independent evidence of periodicity.

CHAPTER 5

CARBON MONOXIDE

5.1 Measurements

Carbon monoxide (CO) concentration measurements were taken for a five minute duration at each monitoring station throughout the experiment (stations A-H; see Fig. 2.2). The resulting chart recording was divided into subsections and the CO concentrations abstracted from the chart by the same method used for the wind speed chart recordings. The five minute series of measurements were then averaged and the resulting concentrations plotted in parts-per-million (ppm). Fig. 5.1 and 5.2 give the resulting CO concentrations from 1700 to 2400 MDT.

Most concentrations, except for those stations close to River Road, were less than 1.0 ppm. Station A did not show any trend in concentration, but varied between 0.0 and 0.8 ppm. Stations B to F showed a rising trend in CO concentration peaking around 2000 MDT. This was in opposition to the pollutant release rate, as the average number of motor vehicles dropped from 1700 per hour at 1730 to 900 per hour at 2000. This indicates that the increase in CO concentration due to the decrease in wind speed prior to the onset of the temperature inversion more than compensated for the emission rate decrease. The CO concentra-

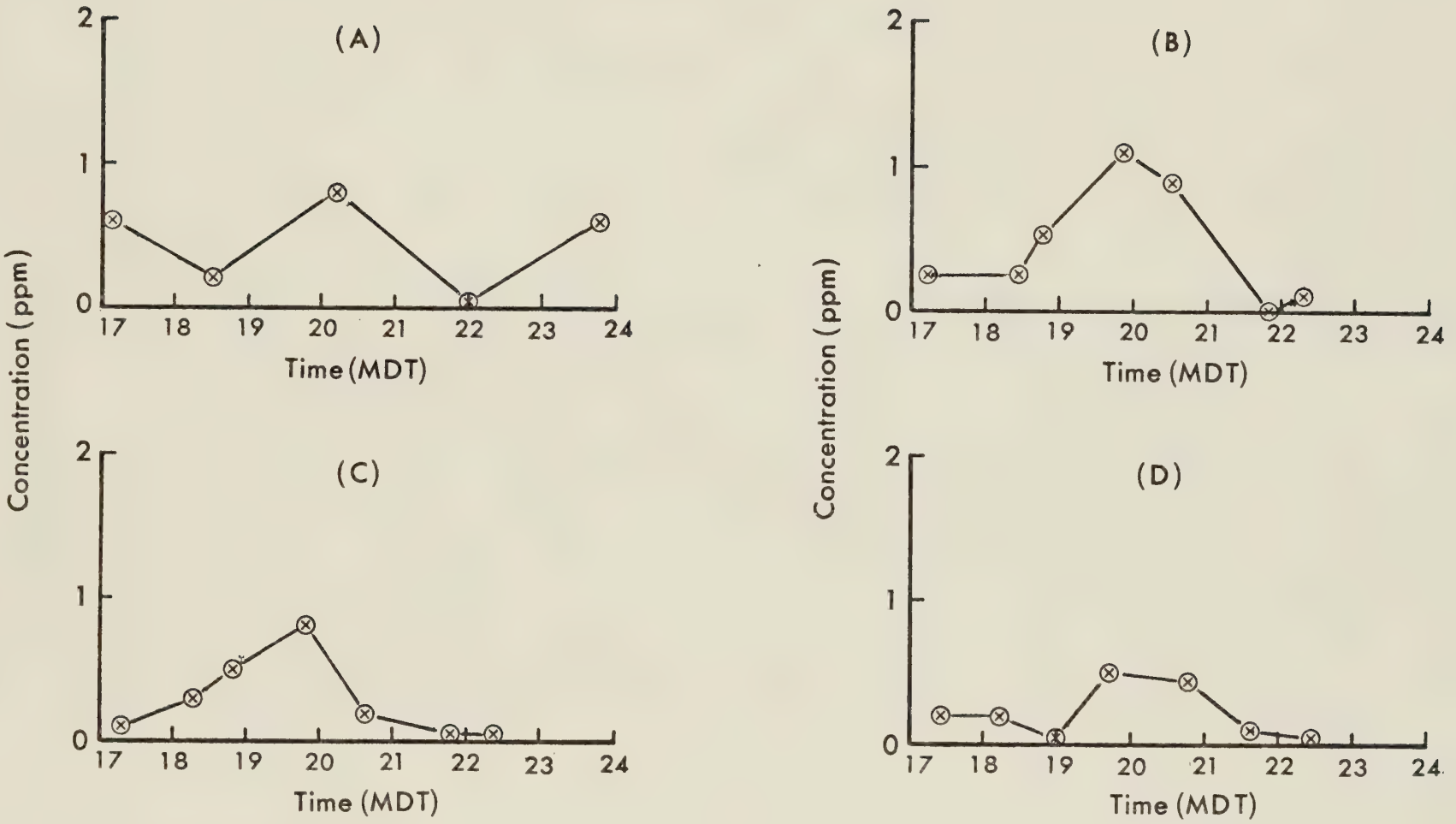

Fig. 5.1. Carbon monoxide concentration at stations A to D.

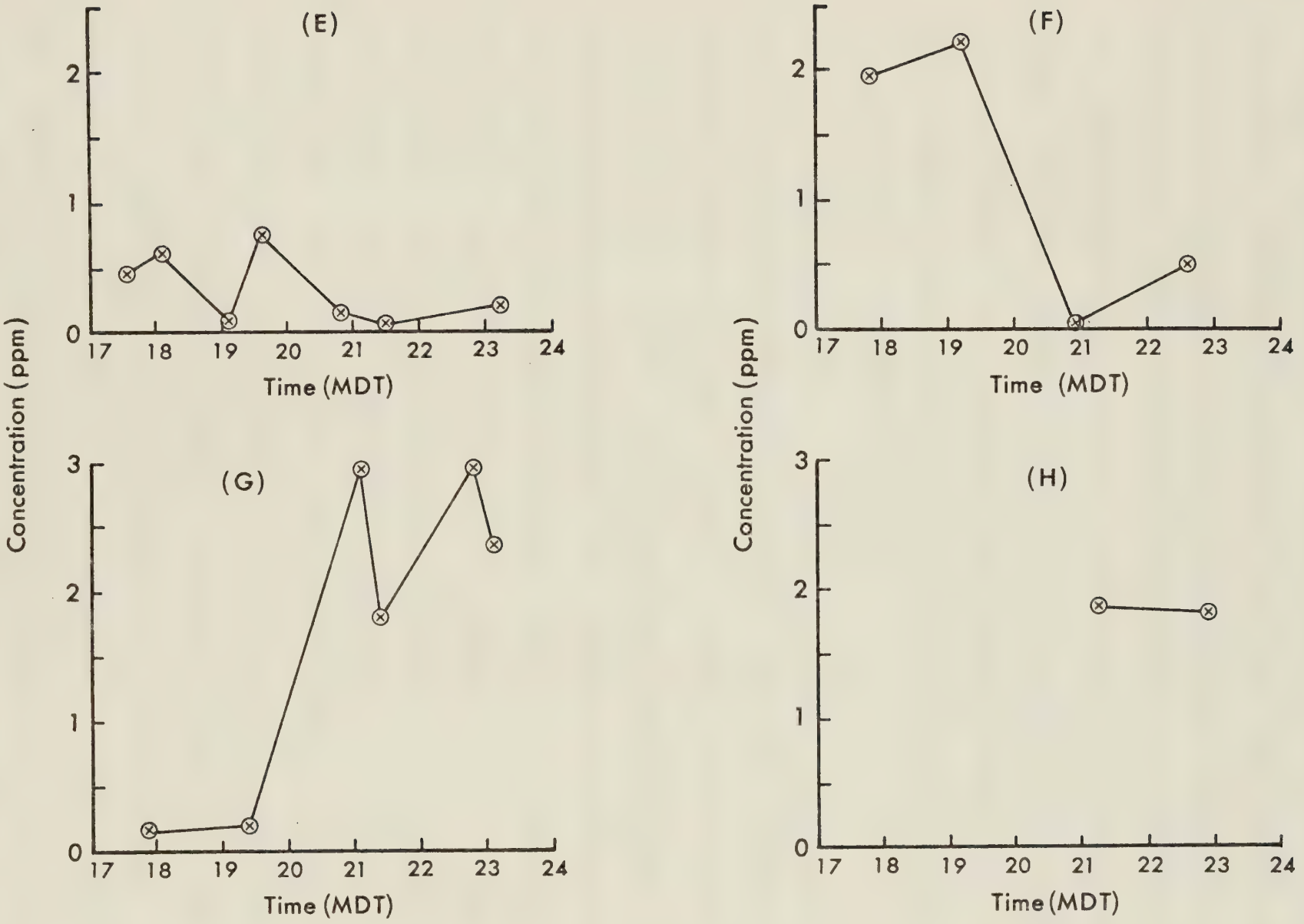

Fig. 5.2. Carbon monoxide concentration at stations E to H.

tions at these stations dropped to average values that were lower after 2000 than before 2000. This was very evident at station E and dramatic at station F where the average concentration dropped from 2.1 ppm before 2000 to 0.2 ppm after 2000. Station 6 showed the opposite trend and, although no measurements were taken at station H until after 2100, the concentrations were in accord with those measured at station 6 after 2100. These trends indicate the effect of the formation of the temperature inversion and the onset of drainage winds.

The concentration at station C peaked at 0.8 ppm before 2000 and decreased by 2035 to 0.2 ppm. Station B showed a peak of 1.2 ppm at 1955, but the concentration was still 0.9 ppm at 2030, indicating that station B must have been within the inversion and came under the influence of the drainage wind later than experienced at station C. This is in agreement with the time taken for the inversion to deepen, as at 2145, when the inversion had filled the valley for one hour, the CO concentration at station B was near zero. The reason for the non-conformity of the time variation of CO concentration at station D has not been explained. Concentrations at station E showed the same time variation as those at station C. This is to be expected, as both stations are close to the same height in the valley. The effect of the drainage flow on CO concentrations was demonstrated most dramatically at stations F and G. These stations were on opposite sides of River

Road. The CO concentration variations were almost mirror images of one another as before 2000 the wind was southerly across River Road and after 2000 was northerly with the onset of the drainage winds. The rapid variation in concentration at station G after 2100 was due to the close proximity of the station to River Road. At short distances single vehicles or groups of vehicles were registered on the CO meter. Station H was far enough away from the road for such variations to be smoothed out.

5.2 Pollution Model

As a quantitative check on the magnitude of the measured CO concentrations, a simple Gaussian plume pollution model was used. For wind direction within 75 degrees to the perpendicular of a highway, Calder (1973) has shown that an approximate expression can be used to determine pollutant concentrations from an infinite line source.

$$\chi_y = \sqrt{\frac{2}{\pi}} \frac{Q}{\bar{U}\, \sigma_z(x) \cos \phi}$$

where χ_y = the concentration at the perpendicular distance y from the highway

$\bar{U}$ = mean wind speed ($m\ s^{-1}$)

Q = emission rate ($g\ m^{-1}\ s^{-1}$)

ϕ = angle from the perpendicular to the highway

$\sigma_z(x)$ = the vertical standard deviation of plume distribution at the downwind distance x, from the source

The vertical standard deviation of plume distribution is an empirical relationship. For $X \leq 0.1$ km and for Pasquill stability class F (moderately stable), Zimmerman (1975) gives the following expression for $\sigma_z(x)$:

$$\sigma_z(x) = 15.209(X + .05842)^{0.81558}$$

where X is in km.

The emission rate Q can be found if the emission factor, EF(g veh^{-1} km^{-1}) and traffic volume, TV(veh hr^{-1}) are known.

$$Q = (EF)(TV)/3600$$

$$= 2.78 \times 10^{-4} (EF)(TV) \ (g\ s^{-1}\ km^{-1})$$

As measurements of wind direction in relation to River Road were not available, a time was chosen when the wind speed measured at station 3 was a minimum. The assumption was made that, in the lower levels over the river valley floor, the wind speed equalled that of the drainage wind. This flow was perpendicular to the road so that $\phi = 0$. The time chosen was 2200 MDT and $\bar{U} \approx 0.4$ m s^{-1} at this time. Alberta Environment[1] lists the emission factor for the average mix

---

[1] Personal communication with A. Schulz, P.Eng., of the Air Pollution Division.

of motor vehicles in Edmonton as EF = 23 g veh^{-1} km^{-1}. Traffic counts made by the City of Edmonton list the average traffic volume at 2200 as TV = 500 veh hr^{-1}, and this was confirmed by an independent count on the night of the experiment. Thus

$$Q = (2.78 \times 10^{-4})(23)(500)$$

$$= 3.2 \text{ g } km^{-1} \text{ } s^{-1}$$

For comparison to the measurements which were in ppm, the calculated concentrations were converted to ppm by

$$\chi(\text{ppm}) = \frac{\chi_y}{\rho_a} = \frac{\chi_y RT}{P}$$

where ρ_a = density of air

P = station pressure at YXD = 9.15×10^4 Pa

T = temperature at 2200 = 275 k

R = gas constant = 287 J kg k^{-1}

Because the vertical standard deviation of plume distribution is a function of stability, concentrations were calculated using the equation for neutral stability to give an indication of the sensitivity of the model to stability. Zimmerman (1975) gives the following expression for $\sigma_z(x)$ for neutral stability:

$$\sigma_z(x) = 34.459(X + .02722)^{.86974}$$

where X is in km.

Using these figures, the results obtained are listed in Table 5.1.

Table 5.1. Comparison between measured and calculated CO concentrations for moderately stable (MS) and neutral stability (N) conditions.

		Concentration (ppm)		
			Calculated	
Station	X(m)	Measured	MS	N
G	33	2.5	2.3	1.7
H	60	1.8	1.9	1.3

The correspondence between the measured and calculated values indicates that the measured values were reasona le. An attempt to calculate CO concentrations before 2000 was not made because the angle of the wind to the perpendicular of River Road precluded the use of this simple model.

CHAPTER 6

SUMMARY AND CONCLUSIONS

During the evening of 21-22 October 1977, an experiment was run to obtain measurements of wind speed, temperature and carbon monoxide concentrations in an effort to determine the micrometeorology of the North Saskatchewan River Valley as it passes through Edmonton, Alberta. The aim of this experiment and a series of others run and planned is to provide the information needed to create a simulation model of the microclimate and pollutant distribution within the river valley. In this experiment, number four of a series, six stations were instrumented on an approximate cross-section of the river valley near the center of Edmonton.

The results of the measurements showed that at 1800 MDT the valley was isothermal up to the rim of the valley and slightly colder than the air above the plain of the city. This was thought to result from the earlier shading of the valley as compared to the plain. The prevailing wind as measured at the municipal airport and on the rim of the valley was from the southeast, and the wind over the river was easterly due to the channeling effect of the valley. The upslope-downslope wind component measured on the north (south facing) slope of the valley indicated up-

slope flow. The temperature at the foot of the south (north-facing) slope was 4°C lower than the rest of the valley due to the earlier onset of cooling of the south slope. The south slope drainage wind was well established by 1830, with no along-valley component evident. By 1930 the temperature profile above the plain (urban profile) was isothermal and the lowest 25 m of the valley showed a slight inversion. The winds above the river were still easterly with a downslope wind component on the north slope. At 2000 an inversion existed in the lowest 14 m of the valley with a temperature gradient of 15°C/100 m. This deepened to fill the valley by 2050, with a gradient of 5.2°C/100 m. The south slope was still colder than the rest of the valley and the resulting gradient, obtained by comparing the south slope station to the valley north rim station, was 13.9°C/100 m. An inversion had formed in the urban air by this time and was less intense than the valley inversion with a gradient of 3°C/100 m. During the time the inversion was filling the valley, the wind above the river had veered from easterly to become westerly, although the prevailing wind remained southeasterly. This was thought to be due to the geometry of the prevailing wind-river valley system, such that the westerly wind in the east-west section of the river valley was a compensating flow between two northerly flowing winds in north-south sections of the valley. After 2050 the wind above the rim of the valley backed to westerly from southeasterly,

apparently in association with the rising inversion. The winds above the valley rim veered back to southeasterly by 2230 and the valley wind was still westerly. The downslope drainage flow was well established on both the north and south slopes of the valley, with the depth of the drainage flow on the north slope at least three metres deep half-way up the slope. The urban inversion gradient was 3.4°C/100 m and in the valley, as measured by the station on the river, the gradient was 6.0°C/100 m, while the gradient measured on the south side was 13.4°C/100 m. This situation remained stable until the conclusion of the experiment. At 2400 the winds were still westerly over the river and downslope on the slopes of the valley. The urban inversion was slightly stronger at 4.6°C/100 m. The inversion gradient over the river was 6.7°C/100 m while over the south slope the gradient was 15.1°C/100 m.

Spectral analysis was performed on the slope winds and on the wind over the river. No evidence of periodicity was found for the valley wind or the north slope drainage wind. There was a periodicity of 15 minutes found in the south slope drainage wind. This was thought to be connected to the wooded nature of the south slope, but independent evidence for its existence was not found in the temperature records.

Carbon monoxide concentrations were measured at several points on the north side of the river (Fig. 2.2). The distribution was found to depend strongly on the wind

field and was seen to decrease north of River Road and increase greatly to the south of River Road with the onset of the drainage wind. Over the flood plain of the river valley, the drainage wind was seen to extend to 15 m in depth by 2400 by observation of plumes emitted from the Glenora Club. A simple pollution dispersion model that assumed an infinite line source and a Gaussian distribution was applied to the vehicle emissions on River Road. Good agreement was found between the measured and theoretical calculations for the case of airflow perpendicular to River Road.

The river station 3 was near the north side of the river and, in the last two hours of the experiment, it showed a northerly wind component. This, along with the drainage flow recorded on the slopes of the valley, implies that the air was converging over the river, and lends support to the concept of a double-vortex circulation within the valley. It was not possible to look for the effect such a circulation would have on the temperature profile measured over the river due to the limitations of the equipment, which ceased functioning before the time any effect would be noticed. The lower temperatures on the south side of the valley could not be maintained with this type of circulation unless there was little interchange of air across the valley and a further study is required to resolve these points.

The results of this study indicate that an inversion

stronger than the urban inversion can form in the valley and that such an inversion is accompanied by a valley wind system. This then has the potential to trap pollutants within the valley, especially on the south side where the inversion is strongest.

REFERENCES

Bergen, J.D., 1969: Cold Air Drainage on a Forested Mountain Slope. J. Appl. Meteor., 8, 884-895.

Calder, K.L., 1973: On Estimating Air Pollution Concentrations from a Highway in an Oblique Wind. Atmos. Environ., 7, 863-868.

Defant, F., 1951: Local Winds. Compendium of Meteorology, Amer. Meteor. Soc., 655-672.

Drinkrow, R., 1972: A Solution to the Paired Gill-Anemometer Response Function. J. Appl. Meteor., 11, 76-80.

Eddy, A., C.E. Duchon and J.A. Alamazan, 1968: Variance Spectrum Analysis. Report No. 8, Atmospheric Science Group, University of Texas.

Fichth, G.H. and Komar, P., 1974: The Response of a Propellor Anemometer to Turbulent Flow with the Mean Wind Vector Perpendicular to the Axis of Rotation. Boundary-Layer Met., 6, 363-380.

Geiger, R., 1965: The Climate Near the Ground. Harvard University Press, Cambridge, Massachusetts, 611 pp.

Gilman, D.L., F.J. Foglister and J.M. Mitchell, Jr., 1963: On the Power Spectrum of "Red Noise". J. Atmos. Sci., 20, 182-184.

Hage, K.D., 1972: Nocturnal Temperatures in Edmonton, Alberta. J. App. Met., 11, 123-129.

Hewson, E.W., 1945: The Meteorological Control of Atmospheric Pollution by Heavy Industry. Quart. J. Roy. Meteor. Sci., 71, 266-282.

Hicks, B.B., 1972: Propellor Anemometers as Sensors of Atmospheric Turbulence. Boundary-Layer Met., 3, 214-228.

Holloway, J.L., Jr., 1958: Smoothing and Filtering of Time Series and Space Fields. Adv. in Geophy., 5, 351-389.

Jenkins, G.M. and D.G. Watts, 1968: Spectral Analysis and Its Applications. Holden-Day, Inc., San Francisco, California, 525 pp.

Julian, P.R., 1971: Some Aspects of Variance Spectra of Synoptic-Scale Tropospheric Wind Components in Mid-Latitudes and in the Tropics. Mon. Wea. Rev., 99, 954-965.

Jung, W.G., 1975: IC Op-Amp Cookbook. Howard W. Sams and Company, Inc., Indianapolis, 591 pp.

Kanasewich, E.R., 1975: Time Sequence Analysis in Geophysics, 2nd edition. University of Alberta Press, Edmonton, 364 pp.

Keeping, E.S., 1962: Introduction to Statistical Inference. D. Van Nostrand Co. Ltd., Princeton, M.J., 451 pp.

Klassen, W., 1962: Micrometeorological Observations in the North Saskatchewan River Valley at Edmonton. Meteorological Branch, Department of Transport, Canada. Technical Circular 3652, 16 pp.

Lachapelle, P.A., 1977: Modern Spectral Methods with Applications to Alberta Climatic Data. M.Sc. Thesis, Department of Geography, University of Alberta, Edmonton.

Madden, R.A., 1977: Estimates of the Autocorrelations and Spectra of Seasonal Mean Temperatures over North America. Mon. Wea. Rev., 105, 9-18.

Meteorology and Atomic Energy, 1968. U.S. Atomic Energy Commission, D.H. Slade, Ed.

Linear Applications, 1973. National Semiconductor Corporation, Marvin K. Vanderkooi, Ed.

Panofsky, H.A., 1973: Tower Micrometeorology in: Workshop on Micrometeorology, Amer. Meteor. Soc., D.A. Haugen, Ed.

_____ and G.W. Brier, 1963: Some Applications of Statistics to Meteorology. Pennsylvania State University, 224 pp.

Paulson, C.A., 1970: The Mathematical Representation of Wind, Speed and Temperature Profiles in the Unstable Atmospheric Surface Layer. J. Appl. Meteor., 9, 857-861.

Sutton, O.G., 1953: Micrometeorology. McGraw-Hill Book Company, Inc., Toronto, 331 pp.

Tang, W., 1974: Mountain-Valley Circulation and Dispersion of Vehicular Exhaust Gases from a Valley Highway. Symposium on Atmospheric Diffusion and Air Pollution, Santa Barbara, California, Sept. 9-13, Published by Amer. Meteor. Soc.

_____, 1976: Theoretical Study of Cross-Valley Wind Circulation. Arch. Met. Geoph. Biokl., Ser. A., 25, 1-18.

Zimmerman, J.R. and R.S. Thompson, 1975: Users Guide for Highway, A Highway Air Pollution Model. U.S. Environmental Protection Agency. Research Triangle Park, North Carolina. Pub. No. 650/4-74-008.

APPENDIX A

TEMPERATURE DATA

This appendix contains the temperatures for all stations used. This includes the Edmonton City Tower temperatures A, B, and C for 10 m, 45.7 m, and 91.4 m respectively.

Table A1. Temperatures at 10-minute intervals for valley stations used in vertical profile.

	Station						
Time	1	4	4a	4b	4c	4d	3
1620	12.2	12.5	10.2	10.2	10.2	10.3	
1630	12.0	12.3	10.6	10.5	10.4	10.5	
1640	11.7	11.9	10.0	10.2	10.1	10.1	
1950	11.7	11.5	10.5	10.2	10.1	10.2	
1700	11.7	11.7	10.5	10.3	10.2	10.3	
1710	11.3	11.1	10.0	10.0	10.0	10.0	
1720	11.3	11.2	10.2	9.9	9.9	9.9	10.5
1730	11.0	11.0	10.1	9.9	10.0	10.0	10.1
1740	10.8	10.7	10.0	10.2	10.2	10.2	9.8
1750	10.5	10.8	9.7	10.0	9.8	9.9	9.8
1800	9.9	10.3	9.6	9.7	9.6	9.6	9.5
1810	10.0	10.0	9.2	9.0	9.0	9.0	9.0
1820	9.1	9.5	8.9	9.0	9.2	9.0	8.5
1830	8.7	8.8	8.6	8.7	8.8	8.8	8.2
1840	8.1	8.5	8.5	8.6	8.7	8.6	7.6
1850	8.0	8.3	8.2	8.1	8.0	8.1	7.6
1900	7.8	8.2	8.0	8.0	7.8	7.7	7.4
1910	7.7	8.1	7.5	7.6	7.4	7.6	7.2
1920	7.6	8.1	7.6	7.6	7.6	7.6	7.2
1930	7.7	7.7	7.1	7.2	7.2	7.1	6.9
1940	7.2	7.6	7.2	7.2	7.2	7.2	7.2
1950	7.0	7.6	7.0	7.1	7.0	6.9	6.0
2000	6.9	7.4	6.7	6.9	6.7	7.0	5.0
2010	6.5	7.3	6.6	6.6	6.6	6.6	4.6

Table A1. Continued.

Time	Station						
	1	4	4a	4b	4c	4d	3
2020	6.4	6.9	6.6	6.2	6.1	6.1	4.0
2030	6.2	7.0	6.5	5.5	5.6	4.5	3.4
2040	5.8	7.0	5.5	4.5	4.6	4.1	3.2
2050	5.3	6.4	4.7	4.5	3.9	3.6	2.9
2100	5.2	6.6	4.6	4.1	3.7	3.6	2.9
2110	5.1	7.0	4.3	3.9	3.6	3.6	2.9
2120	4.8	4.6	4.0	3.9	3.5	3.6	2.4
2130	4.7	4.5	3.5	3.7	3.5	3.1	1.9
2140	4.1	3.3	3.2	3.2			1.6
2150	3.7	3.9	3.1	3.2			1.6
2200	3.7	3.4	3.1	3.1	2.4		1.6
2210	3.4	3.5	3.1	2.9			1.6
2220	3.3	3.7	3.1	2.8			1.6
2230	3.2						1.1
2240	3.1	3.7	2.6	2.4			0.3
2250	3.1						0.2
2300	3.1	3.8					-0.4
2310	3.2	3.8					-0.3
2320	2.8	3.6					-0.6
2330	2.8	2.2					-0.6
2340	2.8	2.2					-0.6
2350	2.7	1.9					-0.9
2400	2.2	1.1					-0.9
0010	1.5	0.9					-0.9

Table A2. Temperatures at 10-minute intervals including Edmonton City Tower

	Station			Tower Level		
Time	2	5	6	A	B	C
1730				10.0	9.5	8.7
1740				9.7	9.3	8.7
1750				9.4	9.1	8.5
1800				9.3	9.0	8.4
1810	8.9			9.1	8.9	8.4
1820	8.7			8.6	8.6	8.1
1830	8.4			8.3	8.3	8.0
1840	7.9	4.7		7.8	7.9	7.7
1850	7.7	4.4		8.2	8.3	8.2
1900	7.4	4.2	8.3	7.5	7.4	7.4
1910	7.4	3.3		7.2	7.3	7.4
1920	7.1	3.1		6.7	7.1	7.7
1930	6.9	3.0	7.3	6.4	6.8	7.5
1940	6.5	2.8		6.1	6.7	7.3
1950	6.3	2.7		5.8	6.4	7.2
2000	5.9	2.6	6.2	5.8	6.3	7.1
2010	6.0	2.4		5.7	6.2	6.7
2020	5.8	2.4		5.6	6.1	6.6
2030	5.3	1.4	4.5	5.3	5.9	6.8
2040	4.3	1.1		5.0	5.8	7.2
2050	3.5	0.8		4.7	5.4	7.3

Table A2. Continued.

	Station			Tower Level		
Time	2	5	6	A	B	C
2100	3.4	0.5	4.4	4.4	5.3	6.9
2110	3.1	0.3		4.4	5.0	6.8
2120	2.9	0.0		4.0	4.9	6.9
2130	2.8	-0.3	3.9	3.8	4.9	6.6
2140	2.5	-0.6		3.6	4.5	6.6
2150	2.4	-0.9		3.4	4.3	6.7
2200	2.2	-0.9	3.3	3.3	4.2	7.3
2210	1.9	-1.2		3.2	3.9	6.7
2220	1.7	-1.4		3.1	3.8	6.3
2230	1.4	-1.4	2.2	3.1	3.9	6.1
2240	1.1	-1.4		2.8	3.7	5.8
2250	1.1	-1.6		2.4	3.6	6.0
2300	1.1	-1.9	1.1	2.2	3.1	6.1
2310	1.1	-2.1		1.9	3.4	5.9
2320	0.7	-2.2		1.7	3.2	5.2
2330	0.3	-2.5		1.7	3.1	5.2
2340	0.3	-2.8		1.4	3.6	5.2
2350	0.0	-2.8		1.4	3.4	5.1
2400	-0.3	-3.0		1.2	3.5	5.3
0010	-0.2	-3.0		1.1	3.3	5.7